B^{11}-Induced Single-Nucleon Transfer Reactions*

J. E. Poth†, J. C. Overley, and D. A. Bromley
Yale University, New Haven, Connecticut
(Received 10 August 1967)

Single-nucleon transfer reactions induced by 115.9-MeV B^{11} ions incident on targets of C^{12}, C^{13}, N^{14}, N^{15}, O^{16}, and Ne^{20} have been studied with the primary objectives of elucidating the reaction mechanism and investigating the utility of such reactions as spectroscopic probes. Reaction-product energy spectra from the (B^{11}, Be^{10}) and (B^{11}, B^{10}) transfer reactions were recorded simultaneously for each target using a dE/dx and E particle identification system which permitted isolation and study of individual residual states. All reactions exhibited highly selective population of residual states, consistent with a particularly simple reaction model involving the direct transfer of a nucleon to an unexcited target core. Evidence was adduced for a mechanism favoring the population of high-angular-momentum states of this configuration. For all targets, ratios of measured cross sections for neutron and proton transfer reactions leading to analog residual states were used to obtain the relative $B^{10}+n$ and $Be^{10}+p$ parentage of the B^{11} ground state on the assumption of charge independence throughout the reactions. Calculations based on available p-shell wave functions were found to be in good accord with the experimental results.

I. INTRODUCTION

THE heavy-ion transfer reaction has been the most extensively studied of the interactions between complex nuclei[1,2]; however, the available data result primarily from such reactions observed at energies below the Coulomb barrier, and in very few cases do they relate to particular residual energy states. The present work is an experimental study of single-nucleon transfer reactions induced by 115.9-MeV B^{11} beams on C^{12}, C^{13}, N^{14}, N^{15}, O^{16}, and Ne^{20} targets. It was undertaken to investigate the reaction mechanism and to determine the extent to which spectroscopic information can be extracted from transfer-reaction cross sections measured at energies significantly above the Coulomb barrier. Data on the (B^{11}, Be^{10}) and (B^{11}, B^{10}) reactions, corresponding to single-proton and single-neutron transfers, respectively, were recorded simultaneously for each target using a particle-identification system capable of resolving both individual residual nuclear species and energy states in these nuclei. Data on the elastic scattering and two-nucleon transfer reactions were also recorded; the (B^{11}, Be^{9}) results will be reported separately.[3]

Recent studies[4,5] of single-nucleon transfer reactions involving heavy-ion projectiles at energies near 10 MeV/amu have demonstrated that, in transfers to strongly populated states, the angular distributions are smoothly varying and display a power-law dependence on linear momentum transfer or, equivalently, an exponential dependence on angle. These results imply that only very limited nuclear-structure information is derivable from transfer angular distributions at these energies. In the present work, therefore, selected angular-distribution data were accumulated to confirm this behavior, while attention was concentrated on the collection of reaction-product energy spectra and on the measurement of absolute cross sections. A detailed analysis of the data from the various targets in terms of the structure of the observed residual states suggests a particularly simple model for these reactions.

The extraction of absolute spectroscopic information from heavy-ion transfer data is at present generally precluded by the lack of detailed nuclear structure calculations for complex nuclei. Recent measurements[5] in the mass-energy region under consideration, however, have demonstrated that cross-section ratios of neutron and proton transfers to two pairs of mirror nuclei in analog states are given correctly in terms of the appropriate isospin Clebsch-Gordan coefficients, implying that it is unnecessary to consider strong isospin admixtures in these reactions. With this assumption, relative spectroscopic factors were extracted from cross-section ratios of (B^{11}, Be^{10}) and (B^{11}, B^{10}) reactions in which only one pair of reaction products is left in analog states. Measurements of such ratios for all targets were used to obtain the relative fractional parentage of the B^{11} ground state based on the low-lying states in Be^{10} and B^{10}, and the results obtained were compared with calculations based on the Kurath[6] and Boyarkina[7] wave functions.

A description of the experimental apparatus and methods is given in Sec. II. In Sec. III the experimental results for the individual targets are presented and discussed as they bear on the reaction mechanism, and in Sec. IV the B^{11} fractional parentage is obtained and compared with the predictions of available model wave-functions. A semiempirical method for calcula-

* Work supported by the U. S. Atomic Energy Commission.
† Present address: Department of Physics, Miami University, Oxford, Ohio.
[1] A. Zucker, Ann. Rev. Nucl. Sci. **10**, 27 (1960).
[2] D. A. Bromley, Brookhaven National Laboratory Report No. BNL 948 (C-46), 1965, Vol. III, p. 1045 (unpublished).
[3] J. E. Poth and D. A. Bromley, Phys. Rev. (to be published).
[4] M. W. Sachs, C. Chasman, and D. A. Bromley, Phys. Rev. **139**, B92 (1965).
[5] J. Birnbaum, dissertation, Yale University, 1966 (unpublished); J. Birnbaum, J. C. Overley, and D. A. Bromley, Phys. Rev. **157**, 787 (1967).
[6] D. Kurath (private communication).
[7] A. N. Boyarkina, Bull. Acad. Sci. USSR, Phys. Ser. **28**, 255 (1964).

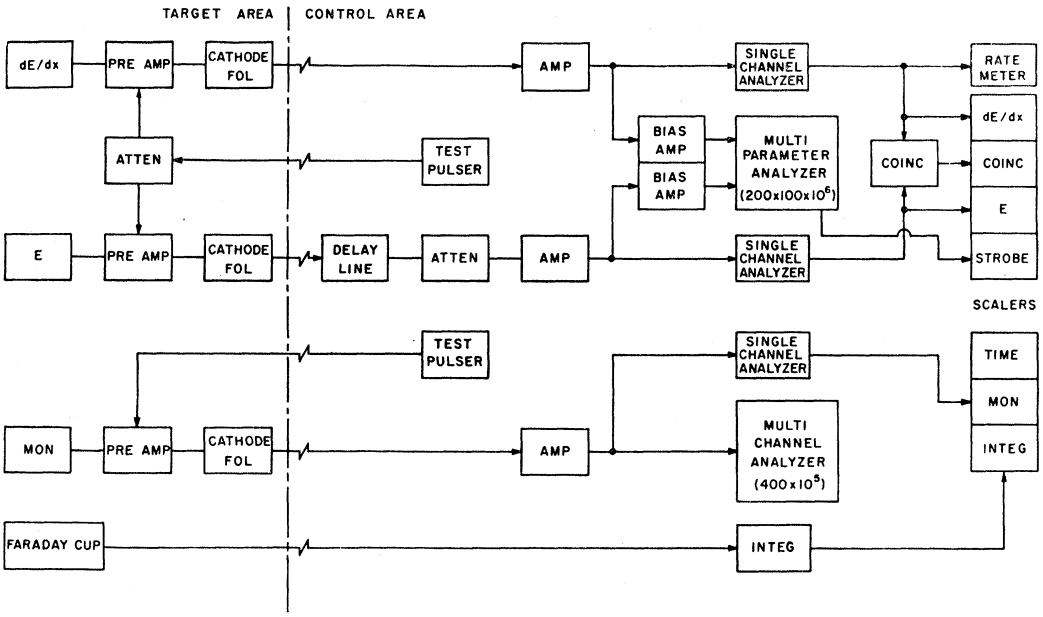

FIG. 1. Block diagram of the electronic system. Impedance matching circuitry is not shown.

tion of energy loss for heavy ions is described in the Appendix.

II. EXPERIMENTAL PROCEDURE

The 115.9-MeV B^{11} beam of the Yale heavy-ion linear accelerator was used throughout this work. After momentum analysis by a previously calibrated magnetic analysis system, the beam entered a 24-in. scattering chamber[8] through two $\frac{1}{8}$-in. collimators and an antiscattering collimator and was collected in a magnetically shielded Faraday cup.

The targets were contained in a gas target cell having 0.000104-in. Havar foil windows. Target pressure was measured with a mercury manometer and temperature was measured with a thermometer system in direct thermal contact with the target cell. The operating pressure was approximately 180 mm Hg (absolute), and the energy losses of the incident beam to target center in the various gases ranged from 0.8 to 1.5 MeV. All targets were obtained commercially. The N_2, O_2, and Ne targets had an analyzed purity in excess of 99.9%; the C target (CH_4) had a nominal purity of 99%. The isotopic purities of the N^{15} target (NH_3) and of the C^{13} target (CH_4) were determined by mass-spectrometer analysis to be 99.2 and 59.1%, respectively.

Reaction products were detected in a dE/dx and E counter telescope[9] consisting of a high-resolution, parallel-plate, gridded ionization chamber transmission counter and a semiconductor residual energy detector. At the chosen operating pressure of 60 in. Hg, the total thickness of the ionization chamber, including the 0.00025-in. Mylar entrance and exit windows, was measured[10] to be 16.9 mg/cm^2 (Al equivalent), corresponding to an energy loss of between 10 and 15% of the energy of the Be and B reaction products. The energy detector was a 3000-Ω cm Au-Si surface barrier detector (Nuclear Diodes) operated at a depletion depth of 550 μ. The energy resolutions of the ionization chamber and energy detector were measured with both the target cell and ionization chamber at operating pressure by scattering 115.9-MeV B^{11} ions from a thin gold target. These resolutions, averaged over all target gases, were 5 and 1%, respectively. The angular aperture of the counter telescope collimation system was $\pm 0.5°$, and the geometric factor[11] for the present work was 8.7×10^{-6} cm. A recirculated-coolant refrigeration system was used on the telescope housing to reduce thermal gain shifts. A 5000-Ω cm Au-Si surface barrier detector operated at a depletion depth of 500 μ was used as a fixed-angle monitor.

A block diagram of the electronic instrumentation is shown in Fig. 1. Preamplification of all detector signals was by thermionic voltage amplifiers; further amplification and single-channel analysis were by transistorized instrumentation.[12] The amplified dE/dx and E signals were applied directly to a 20 000-channel multiparameter pulse-height analyzer (Victoreen, Mod 204 RT) and analyzed in response to an internal 1-μsec coincidence requirement between the two signals. Portions of the dE/dx and E spectra to be analyzed were specified by variable-gain bias amplifiers incor-

[8] C. E. Anderson, A. R. Quinton, W. J. Knox, and R. Long, Nucl. Instr. Methods **7**, 1 (1960).
[9] C. E. Anderson, D. A. Bromley, and M. Sachs, Nucl. Instr. Methods **13**, 238 (1961).
[10] J. E. Poth, dissertation, Yale University, 1966 (unpublished).
[11] E. A. Silverstein, Nucl. Instr. Methods **4**, 53 (1959).
[12] C. E. L. Gingell, IEEE Trans. Nucl. Sci. **NS10**, 32 (1963).

porated in the analyzer input circuitry. Analyzer dead-time measurements were made by scaling an internal voltage signal. The total monitor spectrum was recorded in a multichannel analyzer (RIDL, Mod 34-12B), and the portion of the spectrum used for monitoring purposes was selected by a voltage gate and scaled. System stability was monitored by observation of a precision pulse generator signal applied directly to the preamplifiers. The beam current was adjusted to maintain the average dE/dx counting rate below 330 sec^{-1}; currents were typically 1–5 μA, with a 2% macroscopic duty cycle. Collected beam charge was measured by a commercial integrator (Elcor, Mod A309A).

Particle identification was by the dE/dx and E method. This method utilizes the theoretical formula for the stopping power, which can be expressed [see Eqs. (A1)–(A3)] as

$$-\frac{dE}{dx}=\frac{4\pi e^4 z^{*2}}{m_e v^2}NZ(L+\Delta L), \tag{1}$$

where v and z^*e are the velocity and effective charge of the particle, NZ is the electron density of the absorber, e and m_e are the charge and mass of the electron, L is the stopping number per atomic electron, and ΔL is its relativistic correction. As shown in the Appendix, the effective charge is closely approximated by the nuclear charge ze for the particles and energies utilized in this work, and Eq. (1) can be written, in the nonrelativistic limit, as

$$\frac{dE}{dx}=\frac{Kmz^2}{E}NZL, \tag{2}$$

where m, z, and E are the particle mass, atomic number, and energy, respectively, and K contains only physical constants. The stopping number L has a characteristic logarithmic dependence on particle energy and, in many practical situations, may be considered constant. Equation (2) thus reduces, for a given absorber, to

$$E\frac{dE}{dx}=kmz^2, \tag{3}$$

where k is constant under conditions of negligible energy variation of particle charge and stopping number.

The form of the stopping-power formula given in Eq. (3) is the basis for particle identification in the dE/dx and E method; the identification is absolute for constant k, since no two nuclides have the same value of mz^2. Particles are identified, in general, as hyperbolas in a two-dimensional plot of dE/dx and E or as peaks in the spectrum of their product. In the present system, the hyperbolic loci appear directly as a two-dimensional array in the magnetic core memory of the multiparameter analyzer. The data are available for display during accumulation and are written on computer-compatible magnetic tape for subsequent analysis.

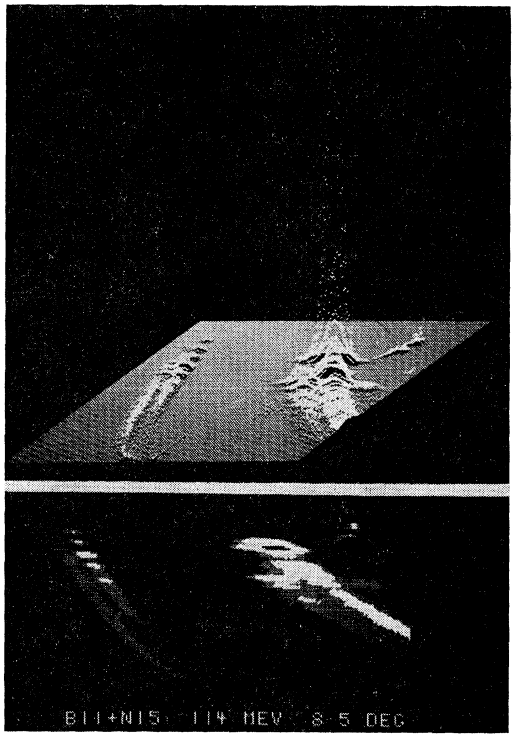

FIG. 2. Multiparameter analyzer CRT displays of dE/dx and E data from the $B^{11}+N^{15}$ reaction. The upper figure is an isometric representation of the analyzer memory, and the lower figure is a contour map of the same data. The dE/dx axis is horizontal in both displays; in each case, the loci at the left correspond to Be^9 and Be^{10}, and those on the right correspond to B^{10}, B^{11}, and B^{12}. The peak at the extreme upper right is an artificially injected calibration pulse. In the contour display, intensity is proportional to yield, with blank areas indicating yields above maximum and below minimum thresholds; yield is shown vertically in the isometric display.

Photographs of typical cathode-ray-tube (CRT) contour and isometric displays for the case of data from the N^{15} target are shown in Fig. 2; these data illustrate the response of the system to the isotopes of Be and B.

The two-dimensional dE/dx and E data were transformed to conventional energy spectra on an IBM 7040/7094 computer. The data-reduction procedure[10] involves least-squares-fitting operations for parametrization of the particle loci and for extraction of experimental yields. For each element analyzed, a generalized form of Eq. (3) is fitted to the locus of each isotope. The resulting parameters locate the loci in a fit of the measured dE/dx detector response function to the data for that element in each plane of constant E. The parameters of this fit give the yield for each isotope at the energy of the plane, and the results for all planes form the one-dimensional energy spectra. The measured E detector response function is fitted to the energy spectra to obtain peak locations and relative populations, which are converted directly to excitation energies and cross sections. The identification system is capable of resolving individual isotopes at least as heavy as those of fluorine. All reaction data are recorded simultaneously for a given

target, so that normalization is not required for comparative measurements.

The energy calibration of the identification system was obtained by elastically scattering the B^{11} beam from a He target. Corrections for energy losses of the beam and of the reaction products in the target cell and ionization chamber were calculated using the method of the Appendix. Absolute differential cross sections were calculated from

$$\left(\frac{d\sigma}{d\omega}\right)_{\text{lab}} = 1.66\times10^{-11}\frac{z^*Y\sin\theta}{GQ(P/T)\eta d}\text{mb/sr}, \quad (4)$$

where θ is the lab scattering angle, z^* is the effective beam charge in units of the charge of the electron, given by the atomic number z in the present measurements, Q is the total integrated beam charge in Coulombs, G is the geometric factor[11] in cm, P and T are the target gas pressure in mm Hg (absolute) and temperature in °K, Y is the experimental reaction yield corrected for analyzer dead time, η is the detection efficiency, and d is the number of atoms of interest per target gas molecule. The estimated error in absolute cross sections and in cross-section ratios is $\pm20\%$. Major contributions to the estimated uncertainty of 1.2 MeV in absolute excitation energies are from the spread in beam energy, uncertainties in the thicknesses of and straggling in the target cell and ionization chamber, and kinematic broadening due to finite detector solid angle. Within this uncertainty, relative excitation energies are determined to within an estimated accuracy of 200 keV.

III. EXPERIMENTAL RESULTS

A. Energy Spectra

The experimental data consist of Be^{10} and B^{10} energy spectra from the various targets and absolute differential cross sections for population of final states corresponding to groups appearing in the spectra. Angular distributions were obtained for several of the reactions; the cross sections decrease smoothly as an exponential function of angle or, alternatively, as a power-law function of linear momentum transfer in accord with previous studies[4,5] of similar heavy-ion systems. Since measurements of this type are capable of providing only very restricted nuclear structure information, only the forward angle spectra and cross sections for each target will be presented and discussed in this section.

Representative energy spectra of the Be^{10} and B^{10} products of (B^{11}, Be^{10}) and (B^{11}, B^{10}) reactions on C^{12}, C^{13}, N^{14}, N^{15}, O^{16}, and Ne^{20} targets are shown in Figs. 3–8, with the Be^{10} spectrum in the upper portion and the B^{10} spectrum in the lower portion of each figure. The data points, error bars, and curves are shown as obtained from the automatic data-reduction procedure described in Sec. II. It should be noted that the error bars reflect not only the usual counting statistics but also any background uncertainties due to adjacent isotopes. The curves in the ranges of excitation energy which contain the major peaks and which will be discussed below are least-squares computer fits to the spectra; at the higher excitations where there are no distinct peaks, the curves simply connect the data points. The abscissa in each case is the multiparameter analyzer E-axis channel number, and the ordinate is the number of counts per channel. The small variation in the laboratory reaction energies reflects the correction applied to the incident beam energy for passage through the gas target cell. All spectra were recorded at the same lab scattering angle of 8.5°, corresponding to c.m. angles between 14° and 16°. The portions of the spectra shown include excitation energies up to approximately 15 MeV; the corresponding range of lab kinetic energies is approximately 70–100 MeV.

The B^{10} and Be^{10} spectra shown in Figs. 3–8 are assumed to arise from proton and neutron transfers, respectively, from projectile to target, rather than from the allowed alternative transfer mechanism often termed backward or heavy-particle stripping.[13] Support for this description and an illustration of the relative importance of the forward and backward stripping amplitudes in heavy-ion reactions have been obtained in a recent study[14] of the $N^{14}+Be^{9}$ system. These results indicate that both amplitudes are present, but that at forward angles such as those considered here, only the forward transfer amplitudes are significant.

The groups appearing in these spectra are interpreted as the excitation of particular states in a binary exit channel. In the discussions of the individual spectra to follow, these states are correlated where possible with known or predicted configurations in order to determine the nature of the transfer mechanism. To facilitate the discussion, an excitation-energy calibration is displayed with each spectrum, and the observed groups will be identified by the excitation energies of the states to which they correspond. The differential cross sections, calculated using Eq. (4), and the excitation energies associated with each group were obtained directly from the data-reduction process. The relative differential cross sections are expected to provide a measure of the relative total cross sections since the similarity of angular distributions characteristic of heavy-ion transfer reactions at these energies makes integration before comparison unnecessary.

The isobaric symmetry of the (B^{11}, Be^{10}) and (B^{11}, B^{10}) reactions is illustrated in the Be^{10} and B^{10} spectra for each target (except N^{15}) by the alignment of intense groups corresponding to analog states in the unobserved residual nuclei. Although primary attention will be focused in this section on the states of these nuclei, it should be noted that the Be^{10} and B^{10} products possess

[13] M. K. Banerjee, in *Nuclear Spectroscopy*, edited by F. Ajzenberg-Selove (Academic Press Inc., New York, 1960), Part B, p. 727.

[14] R. Bock, H. H. Duhm, M. Grosse-Schulte, and R. Rudel, Nucl. Phys. **70**, 481 (1965).

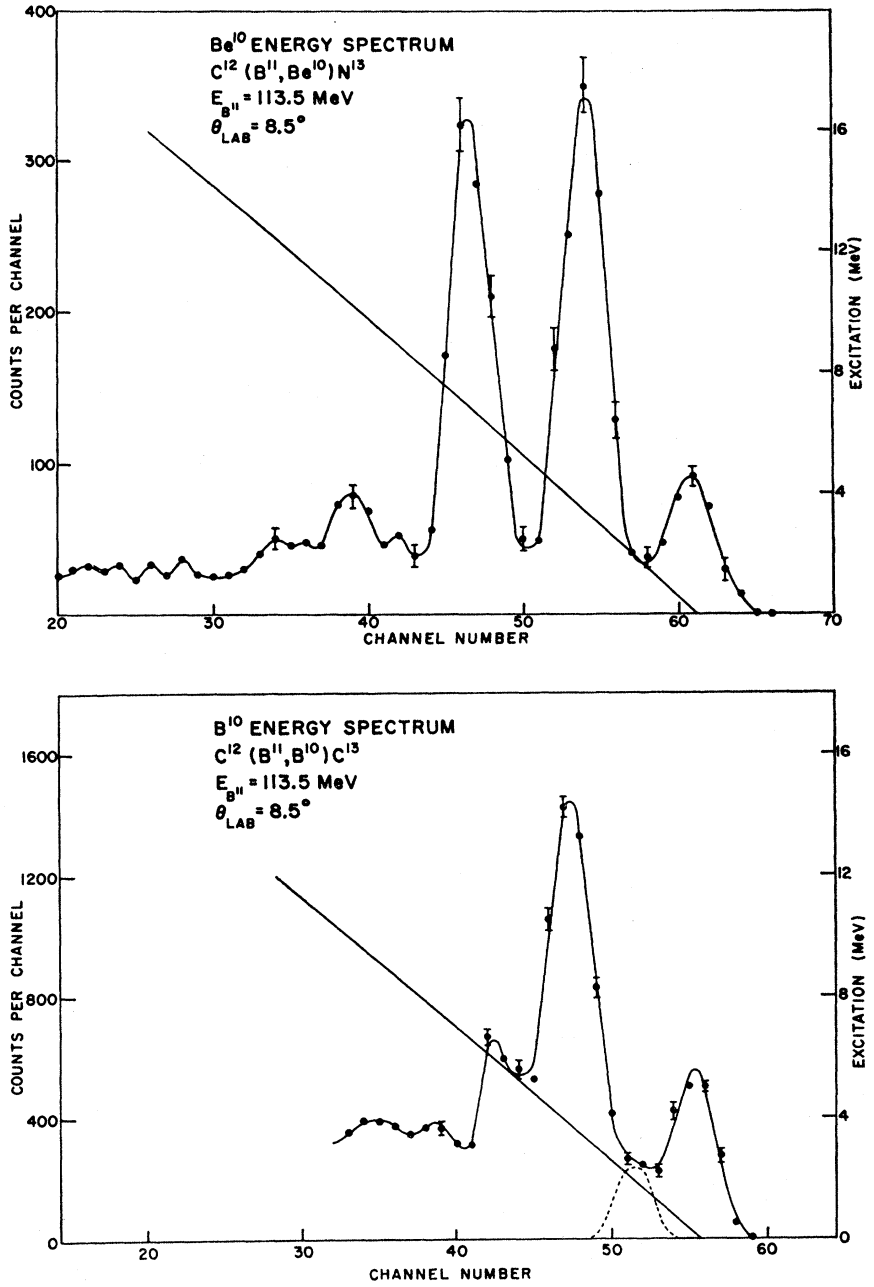

FIG. 3. Be^{10} and B^{10} spectra from a C^{12} target. The solid curves through the distinct peaks to the right of the figure are least-squares computer fits of the E detector response function to the data. To the left of the major peaks, the curve simply connects the data points. The error bars reflect both statistical errors and the quality of the isotopic resolution in a given channel.

low-lying particle-stable states which are also observable. The population of these states reflects the single-nucleon parentage of the B^{11} projectile and will be considered in detail in Sec. IV. Situations in which a given group results from simultaneous excitation of both product nuclei will be referred to as mutual excitations.

The only Be^{10} and B^{10} states which can contribute to the observed spectra are those which lie below the lowest particle-breakup thresholds, if the lifetime of particle unstable states is less than the target-detector flight time. The threshold for the Be^{9}+n breakup of Be^{10} is at 6.814 MeV, thus the first four excited states in Be^{10} at 3.37, 5.96, 6.18, and 6.26 MeV may contribute. States in B^{10} at 0.72, 1.74, 2.15, 3.58, and 4.77 MeV may likewise be involved, since the Li^{6}+α threshold is at 4.463 MeV; the barrier for α-particle emission may also allow the 5.11- and 5.16-MeV states to be observed. The available energy resolution was not sufficient to completely resolve the ground and 0.72-MeV states or the 1.74- and 2.15-MeV states in B^{10}; the ground-state groups in the B^{10} spectra will be assumed to include the 0.72-MeV level in these discussions. The breakup of B^{11} at excitations near 11 MeV into B^{10}+n and Be^{10}+p

has been calculated to be a negligible factor in the interpretation of the spectra in the excitation energy ranges considered.

$$C^{12}(B^{11}, Be^{10})N^{13}$$

The Be^{10} spectrum is shown in Fig. 3. The only distinct groups appear at excitations of 0, 3.5, and 6.9 MeV, with differential cross sections of 0.22, 0.75, and 0.71 mb/sr, respectively. This spectrum is in agreement with that obtained by Sachs *et al.*[4] in a previous investigation.

The 3.5-MeV group corresponds to the 3.37-MeV state in Be^{10} and the 3.51- or 3.56-MeV states in N^{13}. The Be^{10} state probably contributes since this state is observed in all (B^{11}, Be^{10}) reactions studied. A state in N^{13} probably contributes since analysis of the equivalent proton transfer reaction, $C^{12}(He^3,d)N^{13}$ at an incident energy of 25 MeV reveals a corresponding deuteron group.[15] Furthermore, this group has $l=2$ which suggests that the 3.56-MeV, $\frac{5}{2}^+$ state rather than the 3.51-MeV, $\frac{3}{2}^-$ state is involved.

The 6.9-MeV group can result from the mutual excitation of the 3.37-MeV state in Be^{10} and the 3.56-MeV state in N^{13} or from a single excitation in N^{13}. The latter possibility is remote since in the $C^{12}(B^{10}, Be^9)N^{14}$ reaction[4] strong groups are observed only at 0 and 3.5 MeV in the Be^9 ground-state spectrum.

Therefore, the most probable assignments are that the 3.5-MeV group results from Be^{10} in the 3.37-MeV state and N^{13} in the 3.56-MeV state and that the 6.9-MeV group corresponds to mutual excitation of these states. These assignments are consistent with the two-body cluster model of Phillips and Tombrello,[16] which predicts that the ground, 2.37-, 3.56-, and 8.08-MeV states in N^{13} have dominant parentage C^{12}(ground state)$+p$ and that the 3.51-, 6.38-, 6.91-, and 7.40-MeV states are based predominantly on C^{12*} (4.43MeV)$+p$. The $\frac{1}{2}^-$ ground state, the $\frac{1}{2}^+$ state at 2.37-MeV, and the $\frac{5}{2}^+$ state at 3.56 MeV have been identified as the single-particle states in N^{13}, while the 3.51-MeV state is expected to result from the core excitation of a $p_{3/2}$ nucleon.[17] Although the strong excitation of the ground and 2.37-MeV states would also be expected if single-particle states are preferentially populated, there is an apparent inhibition of the population of these low-spin states relative to the 3.56-MeV state. This inhibition will be discussed below.

$$C^{12}(B^{11}, B^{10})C^{13}$$

The B^{10} spectrum is also shown in Fig. 3. A strongly populated group appears at an excitation of 3.8 MeV and weaker groups at 0 and 5.8 MeV. A group at 1.9 MeV is also required to fit the spectrum. The differential cross sections, in order of increasing excitation, are 1.1, 0.42, 3.3, and 1.3 mb/sr.

The $\frac{1}{2}^-$ ground state, the $\frac{1}{2}^+$, 3.09-MeV state, and the $\frac{5}{2}^+$, 3.85-MeV state are the single-particle states in C^{13} and are the mirrors of the N^{13} ground, 2.37-, and 3.56-MeV states, respectively.[17] The cluster-model[16] parentage predictions are C^{12}(ground state)$+n$ for the ground, 3.09-, 3.85-, and 8.33-MeV states and C^{12*}(4.43 MeV)$+n$ for the 3.68-, 6.87-, and 7.68-MeV states. On the basis of the discussion of the $C^{12}(B^{11}, Be^{10})N^{13}$ reaction, the 3.85-MeV state is expected to be strongly populated in this reaction. The 3.8-MeV group corresponds to this state and the 3.58-MeV state in B^{10}; however, the latter state is, in general, formed in low yield in the (B^{11}, B^{10}) reactions studied. This state is also not observably populated in the $B^{11}(p,d)B^{10}$ data of Bachelier *et al.*[18] at $E_p=155$ MeV, and the dominant groups in the deuteron spectrum from this reaction appear at B^{10} excitations of 0, 2.0, 5.0, and 6.9 MeV. Qualitative agreement has been found between these $B^{11}(p,d)B^{10}$ results and the present (B^{11}, B^{10}) data, and similarities in the two reactions will be noted in subsequent discussions.

The most probable assignment for the 3.8-MeV group is the 3.85-MeV, $\frac{5}{2}^+$ state in C^{13}. This assignment is in accord with the $C^{12}(N^{14}, N^{13})C^{13}$ data of Birnbaum *et al.*[5] at an incident energy of 148 MeV. The only strong groups in the N^{13} spectrum from this reaction, with N^{13} detected in the ground state, appear at 0 and 3.8MeV, with a relative intensity approximately equal to that observed in the present work. The group at 1.9-MeV results from the 1.74- and 2.15-MeV states in B^{10}.The 5.18-MeV group may include contributions from the mutual excitation of these states and the 3.85-MeV state in C^{13}.

$$C^{13}(B^{11}, Be^{10})N^{14}$$

The Be^{10} spectrum is shown in Fig. 4. Groups appear at excitations of 0, 3.4, 5.7, 8.8, and 12.2 MeV, with differential cross sections of 0.25, 0.91, 0.84, 2.0, and 0.80 mb/sr, respectively.

The 3.4-MeV group results from the 3.37-MeV state in Be^{10}. The 5.7-MeV group corresponds to the 5.69-MeV, 1^- and 5.83-MeV, 3^- states in N^{14}. The shell-model assignments[19,20] for these states suggest dominant ($p_{1/2}s_{1/2}$) and ($p_{1/2}d_{5/2}$) configurations, respectively, thus their formation in this reaction corresponds to the addition of $s_{1/2}$ and $d_{5/2}$ protons to the C^{13} target core. These states have been found to be strongly populated in the $N^{14}(\alpha,\alpha')N^{14}$ reaction.[21]

The 8.71-MeV, 0^- and 8.91-MeV, 3^- states in N^{14} have likewise been assigned ($p_{1/2}s_{1/2}$) and ($p_{1/2}d_{5/2}$) con-

[15] H. E. Wegner and W. S. Hall, Phys. Rev. **119**, 1654 (1960).
[16] G. C. Phillips and T. A. Tombrello, Nucl. Phys. **19**, 555 (1960); T. A. Tombrello and G. C. Phillips, *ibid.* **20**, 648 (1960).
[17] I. Talmi and I. Unna, Ann. Rev. Nucl. Sci. **10**, 353 (1960).
[18] D. Bachelier, M. Bernas, I. Brissaud, C. Detraz, and P. Radvanyi, J. Phys. (Paris) **24**, 1055 (1963).
[19] W. W. True, Phys. Rev. **130**, 1530 (1963).
[20] E. K. Warburton and W. T. Pinkston, Phys. Rev. **118**, 733 (1960).
[21] B. G. Harvey, J. Cerny, R. H. Pehl, and E. Rivet, Nucl. Phys. **39**, 160 (1962).

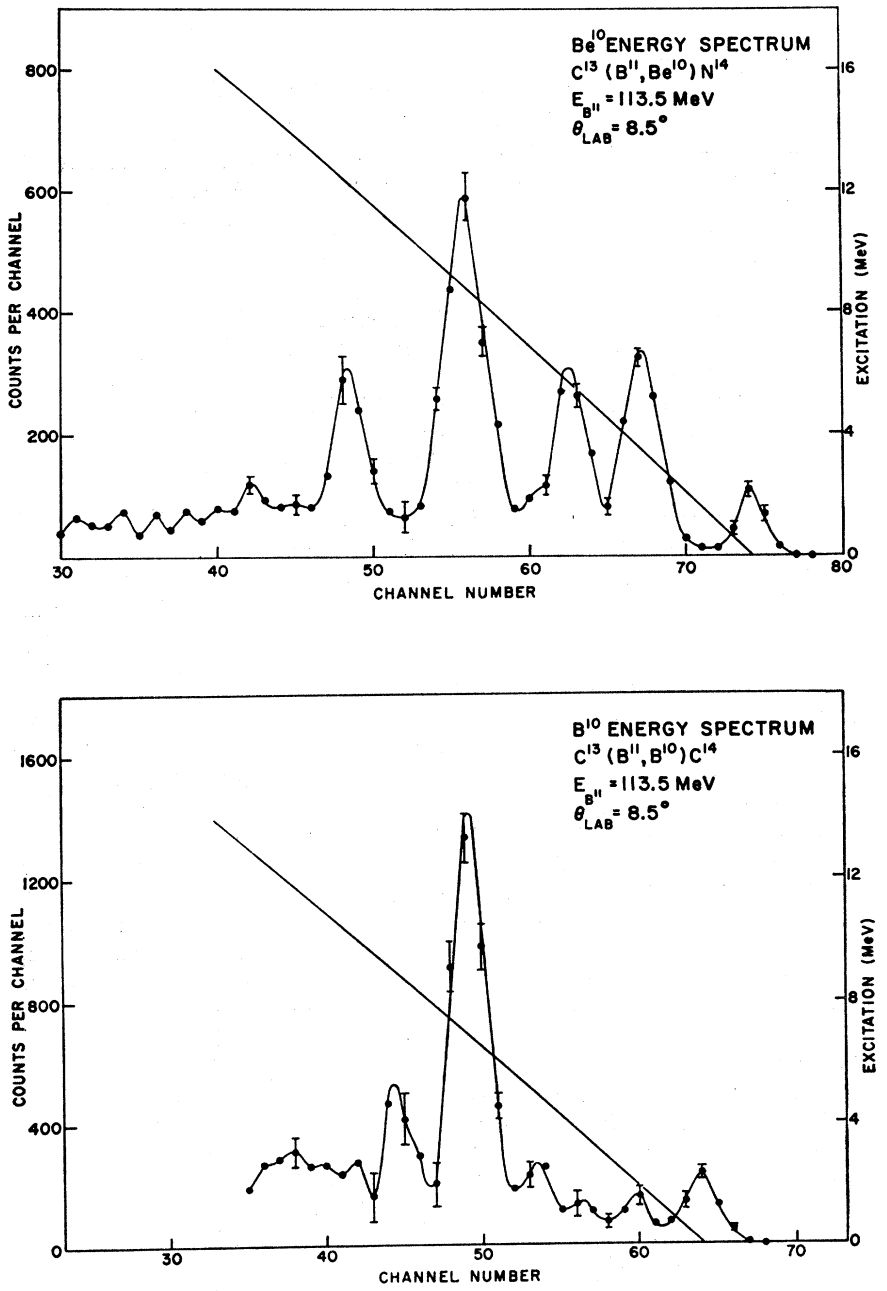

FIG. 4. Be^{10} and B^{10} spectra from a C^{13} target. The significance of the solid curves and error bars is as in Fig. 3.

figurations and are associated with the group at 8.8-MeV, although this group may also contain a contribution from the mutual excitation of states corresponding to the 3.4- and 5.7-MeV groups. The 12.2-MeV group is consistent with either the mutual excitation of the 3.37-MeV state and the states associated with the 8.8-MeV group or from a single excitation in N^{14}. The assignments for the states in N^{14} at 3.95, 6.23, 6.44, and 7.03 MeV indicate that their formation in this reaction would require the excitation of the target core in addition to the transfer of a nucleon. No appreciable population of these states is observed in this work.

This spectrum and the B^{10} spectrum from the $C^{13}(B^{11}, B^{10})C^{14}$ reaction, discussed below, were extracted from those obtained directly from the C^{13} target by subtraction of the corresponding spectra measured with the C^{12} target and normalized to the monitor counter spectrum and the measured C^{12} content of the C^{13} target. The estimated errors for the higher excitations are therefore approximately twice those given in Sec. II.

$C^{13}(B^{11}, B^{10})C^{14}$

The B^{10} spectrum is also shown in Fig. 4. A strongly populated group appears at an excitation of 6.8 MeV, and the weaker groups at 0, 2.0, 3.6, 5.0, and 8.8 MeV. The differential cross sections for the five groups of lowest excitation are 0.55, 0.28, 0.21, 0.71, and 3.8 mb/sr, respectively.

The four groups of lowest excitation result from states in B^{10} and correspond to the removal of a neutron from B^{11} and formation of C^{14} in the ground state, since the first excited state in C^{14} is at 6.09 MeV. The relative populations of these states are in agreement with the $B^{11}(p,d)B^{10}$ data[18] mentioned above.

The 6.8-MeV group corresponds to the 6.72-MeV, 3^- and 6.89-MeV, 0^- states in C^{14} and may be identified with the analog of the state observed at 8.8 MeV in the $C^{13}(B^{11}, Be^{10})N^{14}$ reaction. The 8.8-MeV group most probably results from the mutual excitation of the state associated with the 6.8-MeV group and the 1.74- and 2.15-MeV states in B^{10}.

$N^{14}(B^{11}, B^{10})N^{15}$

The B^{10} spectrum is shown in Fig. 5. A strongly populated group appears at an excitation of 7.2 MeV, and weaker groups at 0, 2.0, 5.2, and 9.2 MeV. The differential cross sections, in order of increasing excitation, are 0.90, 0.46, 0.84, 5.8, and 4.5 mb/sr.

The 2.0-MeV group results from the 1.74- and 2.15-MeV states in B^{10}, since the first excited state in N^{15} is at 5.28 MeV. There is no significant population of the 3.58-MeV state in B^{10}, again in accord with the $B^{11}(p,d)B^{10}$ results.[18]

Halbert and French[22] have carried out intermediate coupling calculations for the even-parity levels in N^{15} and have been able to correlate the observed levels below 9 MeV with dominant $(s^4p^{10}s)$ and $(s^4p^{10}d)$ configurations. The 5.28- and 5.30-MeV states are expected to arise predominantly from the coupling of $d_{5/2}$ and $s_{1/2}$ neutrons, respectively, to an N^{14}, $T=1$ first-excited-state core. The parentage of the 7.16- and 7.57-MeV states and the 7.31- and 8.31-MeV states is predicted to be based primarily on an N^{14} ground-state core, with the former two states having $d_{5/2}$ neutrons and the latter two states having $s_{1/2}$ neutrons coupled to the core. On this basis, the 5.28- and 5.30-MeV states are not expected to be strongly populated in this reaction. The results of the $N^{14}(B^{11}, Be^{10})O^{15}$ reaction to be discussed below and also the $B^{11}(p,d)B^{10}$ data[18] confirm that the main contribution to the 5.2-MeV group results from excitation of a state in B^{10}.

The 7.2-MeV group corresponds to the 7.16-MeV, $\frac{5}{2}^+$ and 7.31-MeV, $\frac{3}{2}^+$ states in N^{15}. The single-particle nature of these states is corroborated by their extremely weak population in the $B^{11}(O^{16}, N^{15})C^{12}$ reaction at an incident energy of 30 MeV.[23] The group at 9.2 MeV may be attributed to the mutual excitation of the state associated with the 7.2-MeV group and the 1.74- and 2.15-MeV states in B^{10} or to a single excitation in N^{15}. The two states arising from the (s^4p^{11}) hole configuration have been associated with the ground, $\frac{1}{2}^-$ and 6.33-MeV, $\frac{3}{2}^-$ states in N.[15,17] There is no evidence for the population of the latter state, consistent with a hole description and its population in the $B^{11}(O^{16}, N^{15})C^{12}$ reaction.[23]

There is good agreement between the present results and those from the $C^{12}(N^{14}, N^{15})C^{11}$ reaction at an incident energy of 148-MeV.[5] The only groups observed in the N^{15} spectrum correspond to states at 0, 2.0, 5.3, 7.3, and 9.4 MeV. The relative intensities of these groups are equivalent in the two cases except for the stronger population of the 5.2-MeV group in the (B^{11}, B^{10}) reaction, further demonstrating that this group is due primarily to a state in B^{10}.

$N^{14}(B^{11}, Be^{10})O^{15}$

The Be^{10} spectrum is also shown in Fig. 5. Groups appear at excitations of 0, 3.4, 5.2, 6.9, and 10.2 MeV, with differential cross sections for the first four of 0.20, 0.49, 0.076, and 0.84 mb/sr, respectively.

The group at 3.4 MeV must result from the 3.37-MeV state in Be^{10}, since the first excited state in O^{15} is at 5.17 MeV. The weak population of the 5.17- and 5.24-MeV states is in accord with the $N^{14}(B^{11}, B^{10})N^{15}$ results discussed above. The strongly populated group at 6.9 MeV corresponds to the 6.85-MeV, $\frac{5}{2}^+$ and 6.79-MeV, $\frac{3}{2}^+$ states in O^{15}, which have dominant single-particle configurations as in the analog situation in N^{15}. The dominant group in the O^{15} spectrum from the $C^{12}(N^{14}, O^{15})B^{11}$ reaction at an incident energy of 148 MeV also appears at this excitation.[5]

The 10.2-MeV group may be identified with a mutual excitation involving the 3.37-MeV state in Be^{10} or with a single excitation in O^{15}. There is no evidence for the formation of the 6.15-MeV analog of the 6.33-MeV state in N^{15}.

$N^{15}(B^{11}, Be^{10})O^{16}$

The Be^{10} spectrum is shown in Fig. 6. Isolated groups appear at excitations of 0, 3.4, 6.1, 9.5, and 12.5 MeV, with differential cross sections of 0.15, 0.52, 0.64, 2.0, and 1.4 mb/sr, respectively.

The 3.4-MeV group again must result from the 3.37-MeV state in Be^{10}, since the first excited state in O^{16} is at 6.05 MeV. The majority of the odd-parity states in O^{16} below 12.5 MeV have been assigned dominant $(p_{1/2}^{-1}s)$ and $(p_{1/2}^{-1}d)$ components in the intermediate shell-model calculations of Elliott and Flowers.[24] The 6.13-MeV state is well represented on this basis as $(p_{1/2}^{-1}d_{5/2})$ and is the most probable assignment for the

[22] E. C. Halbert and J. B. French, Phys. Rev. **105**, 1563 (1957).

[23] R. Bock, M. Grosse-Schulte, W. Van Oertzen, and R. Rudel, Phys. Letters **18**, 45 (1965).

[24] J. P. Elliott and B. H. Flowers, Proc. Roy. Soc. (London) **A242**, 57 (1957).

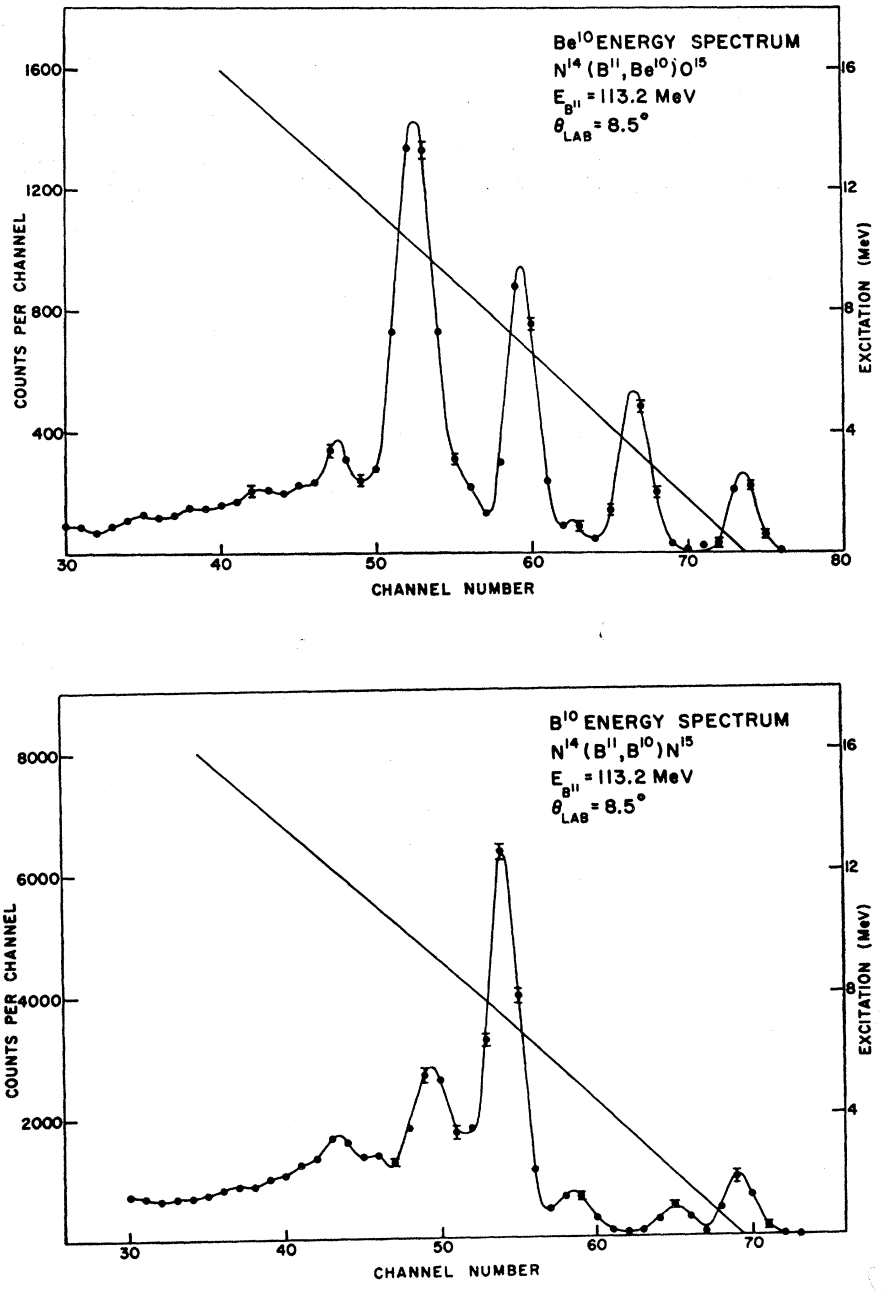

FIG. 5. Be^{10} and B^{10} spectra from an N^{14} target. The significance of the solid curves and error bars is as in Fig. 3.

6.1-MeV group. The calculations of Kelson[25] suggest that the adjacent state at 6.05-MeV results from a two-or-more-particle excitation.

The 9.5-MeV group cannot be uniquely identified as a single excitation in O^{16} or a mutual excitation of the state associated with the 6.1-MeV group and the 3.37-MeV state in Be^{10}. The 9.59-MeV state in O^{16}, which may contribute to this group, may contain a single-particle admixture, but appears to be based primarily on a more complex configuration.[24,25] The 12.5-MeV group corresponds to the 12.44-MeV, 1^- and 12.53-MeV, 2^- states in O^{16}, which have been calculated to have dominant $(p_{1/2}^{-1}d_{3/2})$ configurations, although a mutual excitation cannot be excluded. It would also be tempting to identify this group with the analogs of the four low-lying $T=1$ states in N^{16}, at least one of which is strongly populated in the $N^{15}(B^{11}, B^{10})N^{16}$ reaction discussed below.

$$N^{15}(B^{11}, B^{10})N^{16}$$

The B^{10} spectrum is also shown in Fig. 6. The group of lowest excitation is strongly populated, and weaker groups appear at excitations of 2.0, 3.6, and 5.2 MeV.

[25] I. Kelson, Phys. Letters 16, 143 (1965).

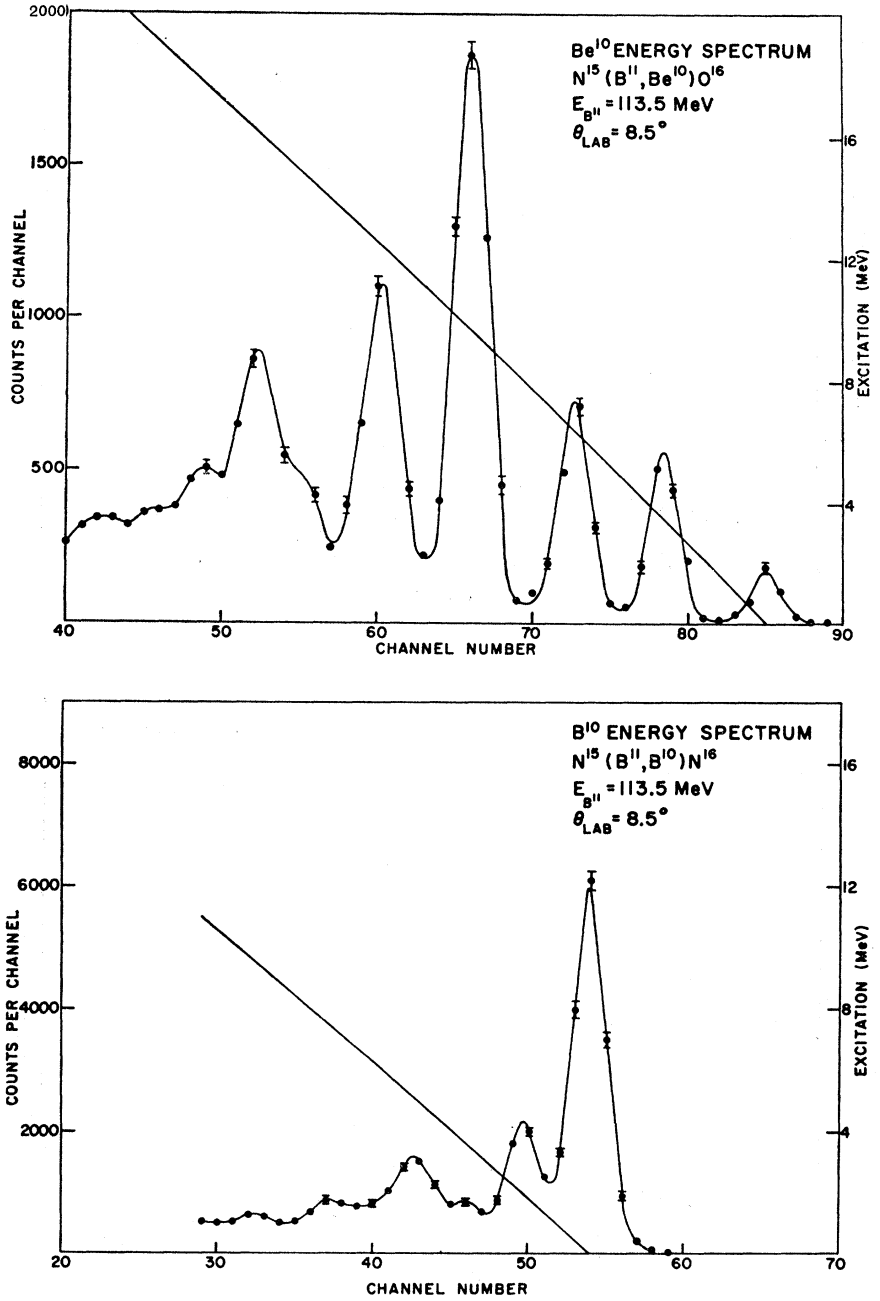

FIG. 6. Be^{10} and B^{10} spectra from an N^{15} target. The significance of the solid curves and error bars is as in Fig. 3.

The differential cross sections are 6.1, 2.2, 0.86, and 2.2 mb/sr, respectively.

The dominant group is obviously complex and corresponds to the excitation of, in addition to the B^{10} ground and first excited states, the ground, 0.12-, 0.30-, and 0.39-MeV, $T=1$ states in N^{16}, all of which are expected[24,25] to arise from $s_{1/2}$ and $d_{5/2}$ single-particle excitations. The 2.0-MeV group results from the 1.74- and 2.15-MeV states in B^{10} and the low-lying quartet in N^{16}.

The weak group at 3.6 MeV corresponds to the 3.58-MeV state in B^{10}. The 5.3-MeV group probably results from an excitation in B^{10} as well as from the broad state at 5.25 MeV in N^{16} corresponding to the strong resonance observed in neutron scattering from N^{15}.

$O^{16}(B^{11}, Be^{10})F^{17}$

The Be^{10} spectrum is shown in Fig. 7. Strongly populated groups appear at excitations of 0 and 3.4 MeV, and weaker groups at 5.5 and 8.6 MeV, with differential cross sections of 1.1, 2.0, 0.46, and 0.75 mb/sr, respectively.

The group at 0 MeV corresponds to the $\frac{5}{2}^+$ ground state and the $\frac{1}{2}^+$ first excited state in F^{17} at 0.50 MeV,

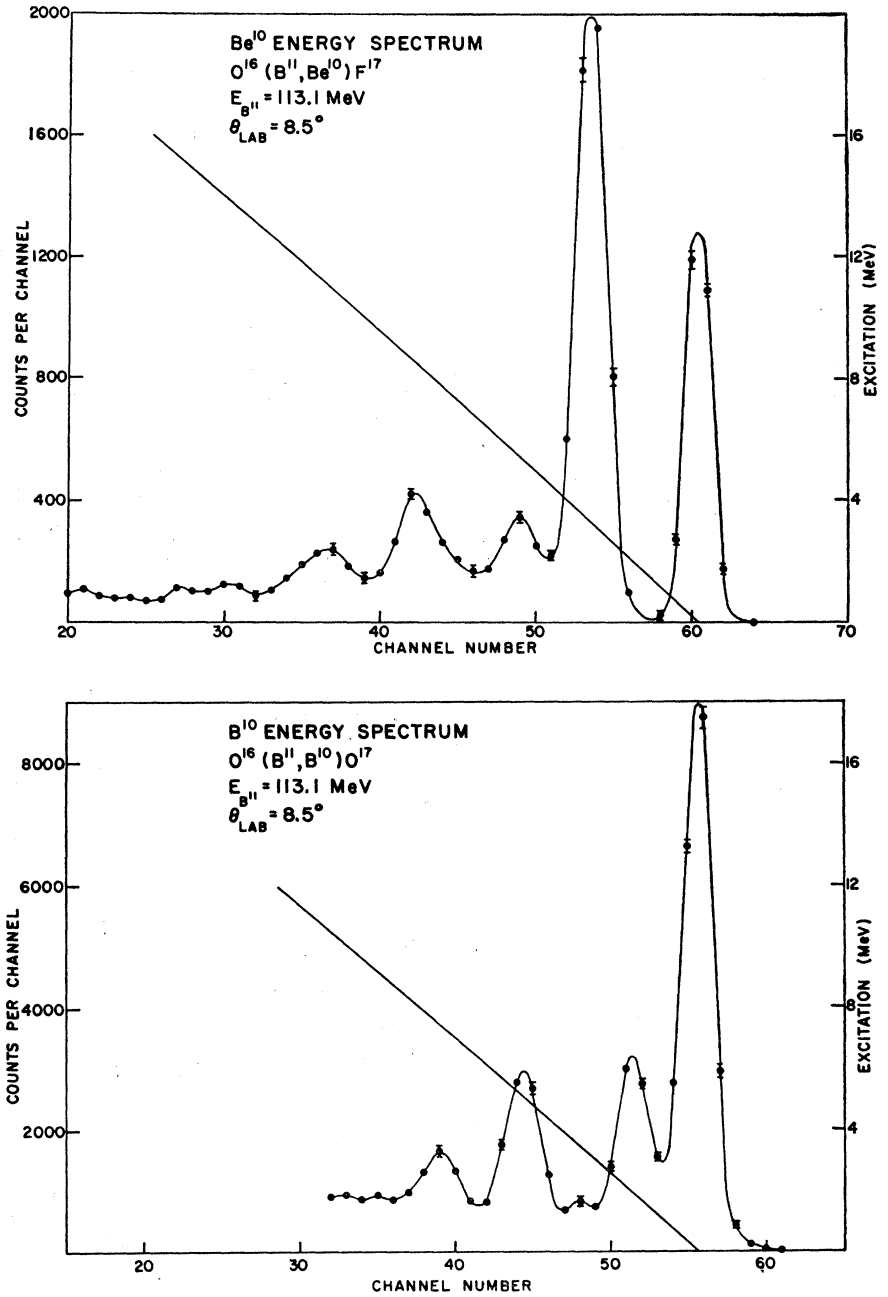

FIG. 7. Be^{10} and B^{10} spectra from an O^{16} target. The significance of the solid curves and error bars is as in Fig. 3.

known to be the $d_{5/2}$ and $s_{1/2}$ single-particle states.[17] The 3.4-MeV group results from the 3.37-MeV state in Be^{10}. Several states in both Be^{10} and F^{17} may be contributing to the weaker groups, and an unambiguous identification cannot be made.

$$O^{16}(B^{11},B^{10})O^{17}$$

The B^{10} spectrum is also shown in Fig. 7. The group of lowest excitation is strongly populated, and weaker groups appear at excitations of 1.9, 3.4, and 5.2 MeV, with differential cross sections of 8.0, 3.4, 0.53, and 3.7 mb/sr, respectively.

The 0-MeV group may be identified with the $\frac{5}{2}^+$ ground state and the 0.87-MeV, $\frac{1}{2}^+$ single-particle states in O^{17}. The 2.0-MeV group results from the 1.74- and 2.15-MeV states in B^{10}. The association of the weak group at 3.4-MeV and the 5.2-MeV group with states in B^{10} is consistent with the results from the $B^{11}(p,d)B^{10}$ reaction.[18]

$$Ne^{20}(B^{11}, B^{10})Ne^{21}$$

The B^{10} spectrum is shown in Fig. 8. Groups appear at excitations of 0, 2.0, 4.7, and 6.6 MeV, with differential cross sections for the three groups of lowest excitation of 4.7, 4.0, and 8.8 mb/sr, respectively.

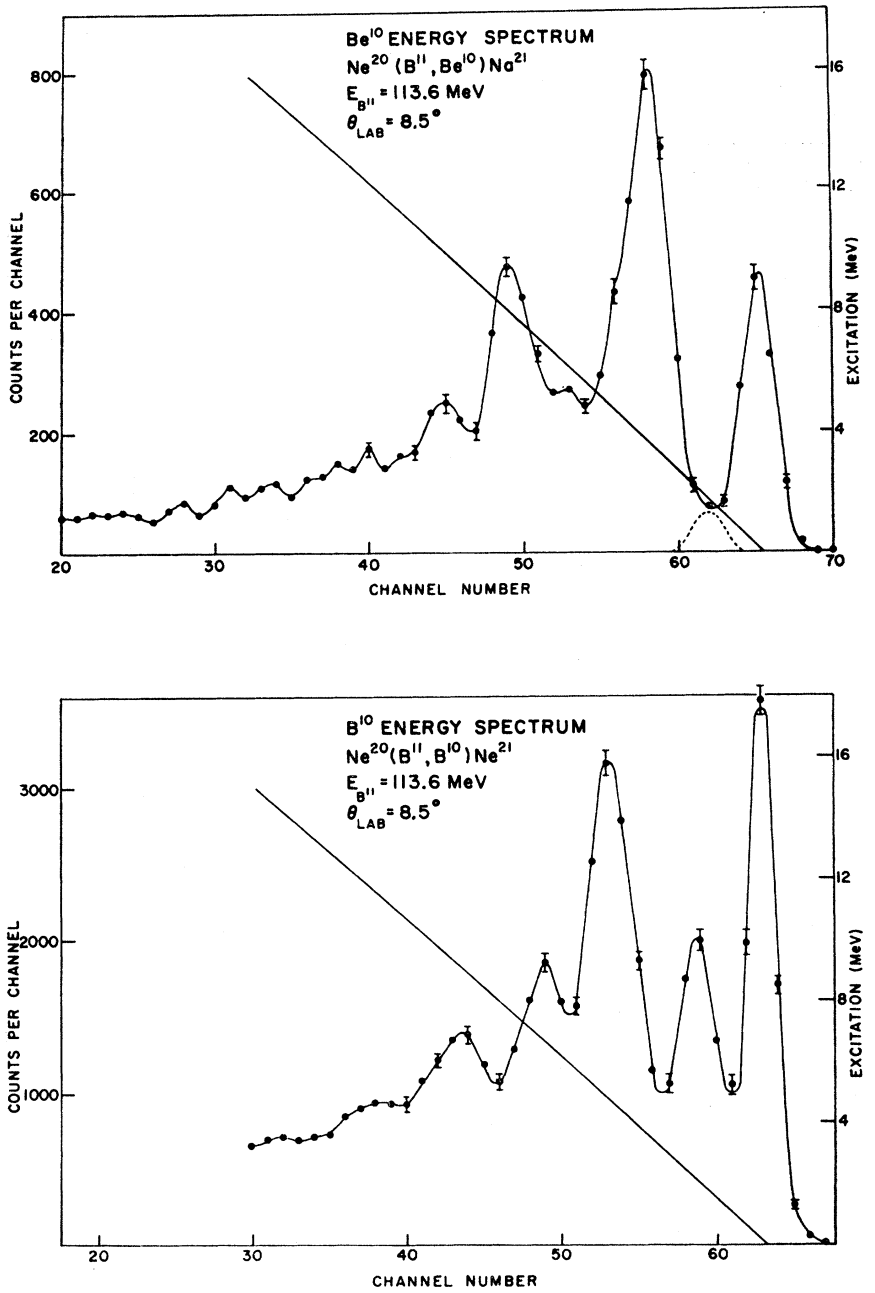

FIG. 8. Be^{10} and B^{10} spectra from a Ne^{20} target. The significance of the solid curves and error bars is as in Fig. 3.

The 0-MeV group corresponds to the $\frac{3}{2}^+$ ground state and the 0.353-MeV, $\frac{5}{2}^+$ first excited state in Ne^{21}. The latter state is strongly populated in the corresponding (d,p) stripping reaction.[26,27] The 2.0-MeV group results from the 1.74- and 2.15-MeV states in B^{10} and from the 1.75-MeV state in Ne^{21}, although the $Ne^{20}(B^{11}, Be^{10})Na^{21}$ results discussed below indicate that the 1.75-MeV state is only weakly excited. The group at 4.7 MeV may result primarily from the 4.73-MeV, $\frac{3}{2}^-$ state in Ne^{21}, also strongly populated in the (d,p) reaction. The 6.6-MeV group contains contributions from the mutual excitation of the state associated with the 4.7-MeV group and the 1.74- and 2.15-MeV states in B^{10}.

$Ne^{20}(B^{11}, Be^{10})Na^{21}$

The Be^{10} spectrum is also shown in Fig. 8. Groups appear at excitations of 0, 3.7, and 7.6 MeV, with differential cross sections for the former two of 0.98 and 2.7 mb/sr, respectively.

[26] H. B. Burrows, T. S. Green, S. Hinds, and R. Middleton, Proc. Roy. Soc. (London) **A69**, 310 (1956).
[27] D. J. Pullen, A. Sperduto, and E. Kashy, Bull. Am. Phys. Soc. **10**, 38 (1965).

The group of lowest excitation may be associated with the ground and 0.335-MeV states in Na^{21}, the mirrors of the ground and first excited states in Ne^{21}. The 1.71-MeV state in Na^{21}, which is the mirror of the 1.75-MeV state is Ne^{21}, is not significantly populated.

The group at 3.7 MeV corresponds to the 3.37-MeV state in Be^{10} and the 4.18-MeV state in Na^{21}, which experimental results[28] suggest to be the mirror of the 4.73-MeV state in Ne^{21}. The data analysis indicates that both states are being populated. The 7.6-MeV group may be attributed to the mutual excitation of the states associated with the 3.7-MeV group.

B. Discussion

Several general characteristics of the (B^{11}, Be^{10}) and (B^{11}, B^{10}) reactions investigated become apparent from consideration of the composite results of the above analysis. The most striking feature is the high degree of selectivity in the population of final states, evidenced by the fact that only a few of the states known to exist in the ranges of excitation energy considered are significantly populated. Another feature is the common excitation of states in the Be^{10} and B^{10} products; for example, the 3.37-MeV state in Be^{10} and the 1.74- and 2.15-MeV states in B^{10} can be clearly seen in all spectra. Mutual excitations involving these states are also evident.

The observed states are correlated, in general, with levels associated with dominant single-particle configurations, while core-excitation states are either relatively weakly populated or not observed. The spectra are therefore consistent with a simple reaction mechanism involving the direct transfer of a single nucleon to a predominantly unexcited target core. The transfer is expected to proceed by means of a surface interaction, since the short mean free paths of both projectile and product in the target nucleus preclude significant contributions from the nuclear interiors. The present data suggest that states are selectively populated having configurations given in jj-coupling notation by $[J_T+(ls)_j]_J$, where the final orbital angular momentum l and s of the transferred nucleon couple to a resultant j, which in turn couples to the spin J_T of the target to form the spin J of the final state.

These reactions are further characterized by the enhanced population of certain of the states which are selectively populated, implying that the single-particle nature of a state is a necessary but not a sufficient condition for its strong population. The appearance of at least one of the preferentially populated levels in each spectrum and the fact that equivalent kinematic conditions are involved in all cases suggest that these states are of a common configuration. This is also indicated by the relationship between the reaction Q values for levels preferentially populated in these reactions and the mass

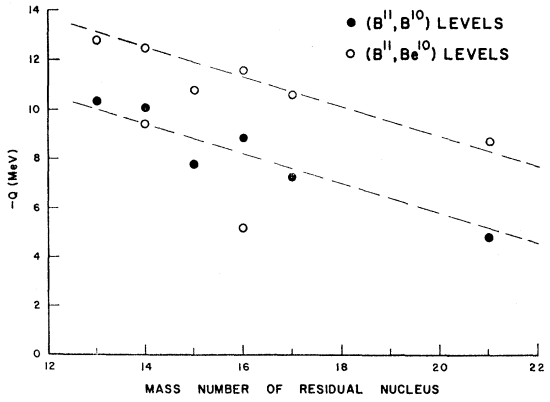

FIG. 9. Dependence of reaction Q value of the mass number of the residual nucleus for levels preferentially populated in (B^{11}, Be^{10}) and (B^{11}, B^{10}) transfer reactions. The dashed lines are arbitrarily drawn.

number of the nuclei in which they are formed, as shown in Fig. 9. The trend toward lower negative Q values, indicated by the arbitrarily drawn dashed lines, suggests that the transferred nucleon is being captured into the same single-particle state, which is such that it approaches the most stable configuration of the residual nucleus as the mass number increases.

The enhancement mechanism is suggested by the fact that each of the levels represented in Fig. 9 is correlated in the previous analyses with a state associated with dominant $d_{5/2}$ single-particle configuration. The preferential population of such states of relatively high angular momentum is expected on the basis of the fact that, at the incident energies of 10 MeV/amu used, each nucleon in the projectile delivers 2–3$\hbar$ of orbital angular momentum to the target surface. On an extreme surface interaction picture, this would be expected to result in enhanced population of states having a configuration $[J_T+d_{5/2}]_J$. Spin-orbit splitting strengths in the sd shell indicate that the corresponding $d_{3/2}$ levels are expected to lie approximately 5 MeV above the $d_{5/2}$ states; the $d_{3/2}$ levels are therefore either not observed or obscured by the inherent mutual excitations.

IV. B^{11} FRACTIONAL PARENTAGE

A. Transfer Cross-Section Ratios

Since the pioneering treatment of stripping reactions by Butler,[29] extensive theoretical studies have been carried out on reactions involving the transfer of a single nucleon between projectile and target nuclei. These investigations have concentrated, in large measure, on situations appropriate to incident deuterons, although interest has recently been focused on such reactions induced by projectiles of mass 3 and 4. The theoretical aspects of heavy-ion transfer reactions have also received considerable attention, dating from the work

[28] A. J. Howard, dissertation, Yale University, 1963 (unpublished).

[29] S. T. Butler, Proc. Roy. Soc. (London) **A208**, 559 (1951).

by Breit and collaborators[30] on the theory of the nucleon tunneling mechanism; the past several years, in particular, have been marked by a significant growth of activity in this field.[31] However, with the exception of tunneling calculations, which are restricted to energies below the Coulomb barrier, a microscopic theory equivalent to that for the lighter projectiles has not yet evolved. Although several current models[32,33] for the transfer reaction at higher incident energies have been found to provide an acceptable qualitative description of available data,[4,5] the wave functions for the heavy nuclei are not yet adequately established to permit the extraction of absolute spectroscopic information on the basis of these model predictions. As will be noted, there is an additional fundamental complication which arises for the heavier projectiles ($A>4$), reflecting the orbital angular momentum of the transferred nucleons while still in the projectile.

To establish notation, a single-nucleon transfer reaction will be described as leading from a projectile a and target A to a product nucleus $a-1$ and a residual nucleus $A+1$. The reaction may be written schematically as

$$a[j_0 t_0 m_0 m_{t_0}]+A[J_0 T_0 M_0 M_{T_0}] \rightarrow (a-1)[j_1 t_1 m_1 m_{t_1}] +(A+1)[J_1 T_1 M_1 M_{T_1}], \quad (5)$$

where the angular momentum and isospin variables have been displayed explicitly. The differential cross section for this process is given in the Born-approximation theory of direct reactions by

$$\frac{d\sigma}{d\omega}=\frac{\mu_i\mu_f}{(2\pi\hbar^2)^2}\frac{k_f}{k_i}\sum|T_{fi}|^2, \quad (6)$$

where T_{fi} is the transition amplitude for the reaction and the summation indicates an average over initial spin states and a summation over final spin states. The reduced masses and relative wave numbers in the initial and final channels are μ_i, k_i and μ_f, k_f, respectively.

The transition amplitude may be written, in general, as a matrix element between product wave functions in the form

$$T_{fi}=\langle\Psi^*(A+1)\Psi^*(a-1)\chi_f^{(-)*} \times|V|\chi_i^{(+)}\Psi(A)\Psi(a)\rangle, \quad (7)$$

where $\chi^{\pm}$ are the scattering wave functions which describe the relative motions of the pairs of nuclei in the initial and final channels, V is the interaction responsible for the transition from the initial to the final state, and the Ψ's are the internal wave functions for the non-interacting separated particles. The nuclear overlap integrals which result from integration over internal coordinates, denoted by ξ, are given by

$$I_1=\int\Psi^*(a-1)\Psi(a)d\xi_{a-1}, \quad (8a)$$

$$I_2=\int\Psi^*(A+1)\Psi(A)d\xi_A. \quad (8b)$$

A convenient method of treating the transition matrix element is to evaluate the overlap integrals by carrying out a fractional parentage expansion of the wave functions $\Psi(A+1)$ and $\Psi(a)$. In such an expansion, an n-nucleon wave function is represented as an expansion in terms of the states of the first $n-1$ particles, with the nth particle being vector coupled to these states. If the state of the transferred nucleon is specified by $(j'l's t)$ while in the projectile and by $(jlst)$ after capture by the target, Eq. (8) becomes

$$I_1=\langle a|a-1\rangle\sum_{j'l'}C(j_1 j' j_0;\, m_1,\, m_0-m_1) \times C(l's j';\, m',\, m_0-m_1-m') \times C(t_1 t t_0;\, m_t,\, m_{t_0}-m_{t_1}) \times\Phi_{l'}{}^{m'}\sigma_s{}^{m_0-m_1-m'}\tau_t{}^{m_{t_0}-m_{t_1}}, \quad (9a)$$

$$I_2=\langle A+1|A\rangle\sum_{jl}C(J_0 j J_1;\, M_0,\, M_1-M_0) \times C(lsj;\, m,\, M_1-M_0-m) \times C(T_0 t T_1;\, M_{T_0},\, M_{T_1}-M_{T_0}) \times\Phi_l{}^{m*}\sigma_s{}^{M_1-M_0-m*}\tau_t{}^{M_{T_1}-M_{T_0}*}, \quad (9b)$$

where Φ, σ, and τ are single-particle wave functions, the Clebsch-Gordan coefficients represent the angular momentum and isospin coupling, and the expansion coefficients are the coefficients of fractional parentage (CFP) connecting the states involved.

It is at this point that an essential simplification occurs if consideration is restricted to projectiles with $A\leq 4$. Under these circumstances, it is reasonable to assume that the transferred nucleon can be represented by an s-wave single-particle wave function, i.e., $l'=0$. The consequences of this become clear if conservation of total angular momentum in the reaction is considered. The orbital angular momentum transfer is given, neglecting spin-flip amplitudes, by the vector coupling of l' and l. If $l'=0$, only a single value l of the angular momentum transfer is involved; however, for situations such as the present case of heavy projectiles in the p shell, several values can contribute, determined by the orbital angular momentum of the transferred nucleon in the projectile and in the residual nucleus.

Straightforward evaluation of the transition matrix element following substitution of the overlap integrals

[30] G. Breit [Phys. Rev. **135**, B1323 (1964)] contains references to earlier work.
[31] K. R. Greider, Ann. Rev. Nucl. Sci. **15**, 291 (1965).
[32] A. Dar and B. Kozlowsky, Phys. Rev. Letters **15**, 1036 (1965).
[33] L. R. Dodd and K. R. Greider, Phys. Rev. Letters **14**, 959 (1965).

given in Eq. (9) leads, in the restricted s-wave case, to the usual factorized expression for the transfer cross section,[34] given by

$$\frac{d\sigma}{d\omega}=\frac{\mu_i\mu_f}{(2\pi\hbar^2)^2}\frac{k_f}{k_i}\frac{(2J_1+1)}{(2J_0+1)}\left|C(t_1tt_0;\, m_{t_1},\, m_{t_0}-m_{t_1})C(T_0tT_1;\, M_{T_0},\, M_{T_1}-M_{T_0})\right|^2 \mathcal{S}(a,\, a-1)\mathcal{S}(A+1,\, A)F_{fi}, \quad (10)$$

where $\mathcal{S}$ is the spectroscopic factor for the indicated transitions and the transfer function F_{fi} is proportional to the absolute square of the transfer amplitude corresponding to a particular orbital angular momentum transfer.

Where more than one value of angular momentum transfer is allowed, this separation of the spectroscopic and transfer contributions into multiplicative factors cannot, in general, be carried out, and the corresponding cross section cannot be evaluated without detailed knowledge of the reaction mechanism and wave functions involved. A different but somewhat parallel difficulty arises in the treatment of multinucleon transfer processes as a result of the coherence between contributions from the various possible configurations of the transferred nucleons.[35] Under these circumstances, it is thus not possible, except in terms of a very specific set of assumptions regarding a nuclear and reaction model, to calculate the transfer function and from it obtain absolute spectroscopic factors from the measured cross section.

Detailed information of this nature is not available for the present reactions, therefore a very approximate method based on the above treatment, involving the extraction of relative spectroscopic factors, has been adopted. In particular, it is assumed that an expression of the form of Eq. (10) will retain approximate validity for the evaluation of transfer reaction data measured under nearly constant kinematic conditions. As usual, it is assumed that the effective transfer function so obtained is relatively insensitive to details of nuclear structure and that such information resides in the spectroscopic factors. The effective transfer function is also considered to remain essentially constant for reactions leading to different states in the same nucleus or to states in adjacent nuclei. It should be emphasized, in support of such an assumption, that transfer reactions proceeding at these energies have been shown to possess similar structureless angular distributions.

Under these assumptions, for a given initial channel leading to neutron and proton transfer final channels, the cross-section ratio can be written as

$$\frac{(d\sigma/d\omega)_n}{(d\sigma/d\omega)_p}=\frac{(k_f)_n}{(k_f)_p}\frac{(2J_1+1)_n}{(2J_1+1)_p}\frac{|C(t_1tt_0;\, m_{t_1},\, m_{t_0}-m_{t_1})C(T_0tT_1;\, M_{T_0},\, M_{T_1}-M_{T_0})|_n^2}{|C(t_1tt_0;\, m_{t_1},\, m_{t_0}-m_{t_1})C(T_0tT_1;\, M_{T_0},\, M_{T_1}-M_{T_0})|_p^2}\frac{(\mathcal{S}(a,\, a-1)\mathcal{S}(A+1,\, A))_n}{(\mathcal{S}(a,\, a-1)\mathcal{S}(A+1,\, A))_p}. \quad (11)$$

The further application of this expression is dependent on the extent to which the reactions involved can be considered to be charge independent; relevant transfer reaction data have been obtained in a recent study[5] of the $N^{14}+C^{12}$ system at an incident energy of 148 MeV. Measurements on neutron and proton transfer reactions leading to mirror states in both final channels, i.e., where $(\mathcal{S}(a,\, a-1)\mathcal{S}(A+1,\, A))_n=(\mathcal{S}(a,\, a-1)\mathcal{S}(A+1,\, A))_p$, have demonstrated that cross-section ratios predicted on the basis of pure isospin are in good agreement with the experimental ratios. With the assumption that this result can be extended to similar heavy ion systems, it is possible to evaluate directly the isospin Clebsch-Gordan coefficients appearing in Eq. (11) for final states populated in the present reactions.

For cases in which analog or mirror states are populated in the $(A+1)$ nuclei following neutron and proton transfer, the corresponding spectroscopic factors are necessarily equal, and Eq. (11) reduces to

$$\frac{(d\sigma/d\omega)_n}{(d\sigma/d\omega)_p}=\frac{(k_f)_n}{(k_f)_p}\frac{|C(t_1tt_0;\, m_{t_1},\, m_{t_0}-m_{t_1})C(T_0tT_1;\, M_{T_0},\, M_{T_1}-M_{T_0}|_n^2}{|C(t_1tt_0;\, m_{t_1},\, m_{t_0}-m_{t_1})C(T_0tT_1;\, M_{T_0},\, M_{T_1}-M_{T_0})|_p^2}\frac{(\mathcal{S}(a,\, a-1))_n}{(\mathcal{S}(a,\, a-1))_p}. \quad (12)$$

Evaluation of the isospin coefficients permits extraction of empirical spectroscopic factor ratios from the measured cross sections. These results can then be compared with ratios calculated on the basis of specific model wave functions using, for example, the formalism developed by Macfarlane and French.[36]

For wave functions given in an LS representation specified by (αLST), where α denotes the space symmetry of the orbital component, the spectroscopic factor may be expressed as

$$\mathcal{S}=n\sum_z|I(z)|^2, \quad (13)$$

where z is the channel spin and n is the number of nucleons in the initial state identical to the transferred nucleon. The overlap integral $I(z)$ is given by

$$I(z)=\langle\Psi(\alpha LST)|[\Phi(\alpha_0L_0S_0T_0)+\Phi(l)]\rangle, \quad (14)$$

[34] See, for example, J. B. French, in *Nuclear Spectroscopy*, edited by F. Ajzenberg-Selove (Academic Press Inc., New York, 1960), Part B, p. 890.

[35] N. K. Glendenning, Phys. Rev. **137**, B102 (1965).

[36] M. H. Macfarlane and J. B. French, Rev. Mod. Phys. **32**, 567 (1960).

where Ψ and Φ are the initial- and final-state wave functions, respectively, and $\Phi(l)$ is the wave function of the transferred nucleon, which is coupled as indicated to Φ. This overlap integral may be evaluated by a fractional parentage expansion of Ψ, with the expansion coefficients being the CFP connecting the states (αLST) and $(\alpha_0 L_0 S_0 T_0)$. The state wave functions are usually given as linear combinations of basic model wave functions in the form

$$\Psi_{JT}=\sum_{\alpha LS} K_{\alpha LS}{}^{J}\Psi_{\alpha LST}, \tag{15a}$$

$$\Phi_{J_0T_0}=\sum_{\alpha_0 L_0 S_0} K_{\alpha_0 L_0 S_0}{}^{J_0}\Phi_{\alpha_0 L_0 S_0 T_0}. \tag{15b}$$

Equation (14) thus becomes

$$I(z)=\sum_{\substack{\alpha LST,\\ \alpha_0 L_0 S_0 T_0}} K_{\alpha LST}{}^{J}K_{\alpha_0 L_0 S_0 T_0}{}^{J_0}(-1)^{l+L_0+L} \times\langle\alpha LST|\alpha_0 L_0 S_0 T_0\rangle U(lL_0JS:Lz) \times U(L_0 S_0 zs:J_0 S), \tag{16}$$

where $\langle\alpha LST|\alpha_0 L_0 S_0 T_0\rangle$ are the CFP and the U's are the normalized Racah coefficients[37] required to specify J_0 and z in the channel spin representation. In the calculations, the CFP for the p shell were taken to be those given by Jahn and Van Wieringen,[38] as amended by Elliot *et al*[39]; the U coefficients were evaluated using a standard tabulation[40] of the Racah W coefficients.

B. Results and Discussion

The (B^{11}, B^{10}) and (B^{11}, Be^{10}) reactions may be written schematically for a target A as

$$B^{11}+A=(B^{10}+n)+A\rightarrow B^{10}+(A+n), \tag{17a}$$

$$=(Be^{10}+p)+A\rightarrow Be^{10}+(A+p). \tag{17b}$$

This notation illustrates the isobaric symmetry of the two pairs of residual nuclei and reflects the initial and final system parentages represented by the spectroscopic factors appearing in the cross section relation for these processes. The ratio of cross sections of neutron and proton transfers to analog or mirror states in the $(A+n)$ and $(A+p)$ nuclei and to arbitrary states in B^{10} and Be^{10} is of the form given in Eq. (12) and may be expressed using the above notations as

$$R=\frac{(d\sigma/d\omega)_n}{(d\sigma/d\omega)_p}\frac{(k_j)_p}{(k_j)_n}=\frac{[C(B^{10}+n)C(A+n)]^2}{[C(Be^{10}+p)C(A+p)]^2} \times\frac{\mathcal{S}(B^{10}+n)}{\mathcal{S}(Be^{10}+p)}. \tag{18}$$

The cross-section ratios defined by Eq. (18) have been considered in four cases involving low-lying states in B^{10} and Be^{10}. For the numerators of the ratios, R_1 involves the sum of the ground state and 0.72-MeV state of B^{10}, R_2 involves the 1.74-MeV and 2.15-MeV states of B^{10}, R_3 involves the 3.58-MeV state of B^{10}, and R_4 involves the 3.37-MeV state of Be^{10}. Experimental ratios have been derived from the cross-section data presented in Sec. III for each target for which isolated groups corresponding to the indicated excitations appear in the energy spectra.

Following evaluation of the appropriate isospin Clebsch-Gordan coefficients, the ratios are given by

$$R_1=\frac{3}{2}\frac{\mathcal{S}(B^{10}(\text{g.s.})+n)+\mathcal{S}(B^{10}(0.72\text{ MeV})+n)}{\mathcal{S}(Be^{10}(\text{g.s.})+p)}, \tag{19a}$$

$$R_2=\frac{\mathcal{S}(B^{10}(1.74\text{ MeV})+n)+3\mathcal{S}(B^{10}(2.15\text{ MeV})+n)}{\mathcal{S}(Be^{10}(\text{g.s.})+p)}, \tag{19b}$$

$$R_3=\frac{\mathcal{S}(B^{10}(3.58\text{ MeV})+n)}{\mathcal{S}(Be^{10}(g.s.)+p)}, \tag{19c}$$

$$R_4=\frac{\mathcal{S}(Be^{10}(3.37\text{ MeV})+p)}{\mathcal{S}(Be^{10}(\text{g.s.})+p)}. \tag{19d}$$

These values are for reactions proceeding from $T=0$ target nuclei to $T=\frac{1}{2}$, $T_z=\pm\frac{1}{2}$ analog or mirror states; equivalent expressions hold for reactions proceeding from $T=\frac{1}{2}$ target nuclei to $T=1$, $T_z=0,1$ analog states.

A comparison of experimental and calculated values of the cross-section ratios R_1, R_2, R_3, and R_4 is given in Table I. The use of a variety of targets permits the same ratio to be obtained in several reaction situations; the internal consistency of the experimental results provides support for the approximations inherent in the present analysis. The calculated ratios were obtained from the Kurath wavefunctions.[6] Calculations based on the intermediate coupling LS wave functions of Boyarkina[7] using Eqs. (13) and (16) yield similar results; for example, R_1 and R_2 were calculated to be 4.26 and 1.83, respectively.

The relative fractional parentage of the B^{11} ground state based on low-lying states in Be^{10} and B^{10} has been obtained from the average experimental values given in Table I on the basis of Eq. (19) by normalizing to the spectroscopic factors for the ground and 0.72-MeV states in B^{10}. The independence of the spectroscopic factors on the third component of isospin permits their extraction for the unresolved 1.74- and 5.16-MeV states in B^{10} from the data on the isolated ground and 3.37-MeV states in Be^{10}, respectively. The experimental relative spectroscopic factors are compared with those calculated from the Kurath wave functions[6] in Table II; the Boyarkina wave functions[7] again give essentially

[37] H. A. Jahn, Proc. Roy. Soc. (London) **A205**, 192 (1951).
[38] H. A. Jahn and H. Van Wieringen, Proc. Roy. Soc. (London) **A209**, 502 (1951).
[39] J. P. Elliott, J. Hope, and H. A. Jahn, Phil. Trans. Roy. Soc. **A246**, 241 (1953).
[40] A. Simon, J. H. Vander Sluis, and L. C. Biedenharn, Oak Ridge National Laboratory Report No. ORNL-1679, 1954 (unpublished).

TABLE I. Comparison of calculated and experimental (B^{11},B^{10}) and (B^{11},Be^{10}) transfer reaction cross section ratios. All ratios are relative to Be^{10}(g.s.) and are identified by $R_1=B^{10}$(g.s.) $+B^{10}$(0.72 MeV), $R_2=B^{10}$(1.74 MeV)$+B^{10}$(2.15 MeV), $R_3=B^{10}$-(3.58 MeV), $R_4=Be^{10}$(3.37 MeV).

Target	R_1	R_2	R_3	R_4
C^{12}	4.96	1.90		
C^{13}	3.96	2.01		3.73
N^{14}	4.41	2.26	0.59	2.51
N^{15}				3.45
O^{16}	7.32	3.18	0.50	
Ne^{20}	4.63	3.26		
Average	5.06	2.52	0.55	3.23
Calculated	3.15	1.75	0.61	2.64

equivalent values. The relative ($B^{10}+n$) and ($Be^{10}+p$) parentage of the B^{11} ground state represented by these results is displayed in Fig. 10. The agreement between calculations and experiment provides additional evidence that available p-shell wave functions realistically represent nuclei in the beryllium-boron region.

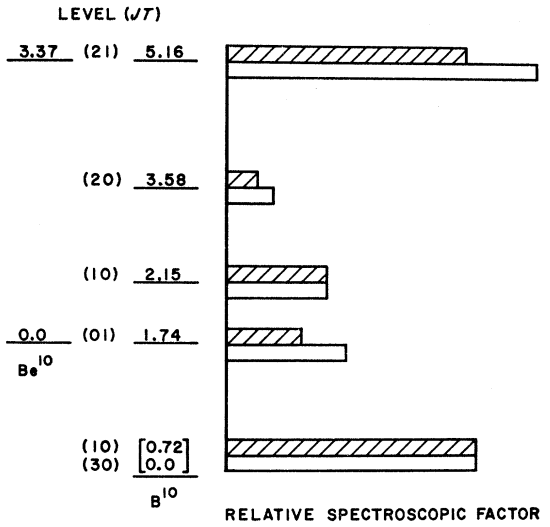

FIG. 10. Relative $B^{10}+n$ and $Be^{10}+p$ parentage of the B^{11} ground state. Low-lying levels in B^{10} and their analogs in Be^{10} are shown vertically. The corresponding experimental (shaded) and calculated (open) relative spectroscopic factors are shown horizontally.

V. SUMMARY

Single-nucleon transfer reactions induced by 115.9-MeV B^{11} beams have been studied with a series of light targets ranging from C^{12} to Ne^{20}. All reactions exhibit highly selective population of final states, and a detailed analysis of reaction product energy spectra suggests a particularly simple reaction model. The strong population of states of a dominant single-particle nature and the weak population or absence of states whose formation would involve core excitation in addition to the transfer process indicate that states are selectively populated which have strong parentage based on the transferred nucleon coupled to an unexcited target core. The data are consistent with the preferential population of states of dominant $d_{5/2}$ single-particle configurations, as expected on the simplest classical representation of the transfer reaction at these incident energies.

Measurement of cross-section ratios of neutron and proton transfer reactions leading to analog or mirror states in the target plus nucleon final systems has permitted the extraction of relative spectroscopic factors for the incident B^{11} single-nucleon systems. These data have been used to obtain the relative fractional parentage of the B^{11} ground state based on low-lying states in Be^{10} and B^{10}. Calculations of this parentage based on available p-shell wave functions have been found to be in good accord with the experimental results. The utility of the transfer reaction as a spectroscopic probe has been demonstrated through the development of instrumentation which permits the isolation and study of individual residual energy states. Extensions of these studies with higher-resolution variable-energy heavy-ion beams will be of considerable interest.

TABLE II. Comparison of experimental and calculated relative spectroscopic factors for low-lying levels in B^{10} and Be^{10}.

Level (MeV)			Relative spectroscopic factor	
B^{10}	Be^{10}	(JT)	Experiment	Calculated
0.0		(30)		
0.72		(10)	1.00	1.00
1.74	0.0	(01)	0.30	0.48
2.15		(10)	0.40	0.40
3.58		(20)	0.12	0.19
5.16	3.37	(21)	0.96	1.26

ACKNOWLEDGMENTS

The authors are indebted to Dr. J. Birnbaum for assistance in the development of the techniques utilized herein and in the collection of the experimental data, to Dr. K. Nagatani for sharing in the data taking, to Dr. L. C. Northcliffe for helpful discussions on the range-energy calculations and for use of his unpublished data, and to Dr. D. Kurath for communication of results of his calculations prior to publication. We acknowledge the assistance of C. E. L. Gingell with the electronic instrumentation and thank the staff of the Yale heavy-ion linear accelerator under the direction of Professor E. R. Beringer.

APPENDIX: SEMIEMPIRICAL CALCULATION OF ENERGY LOSS FOR HEAVY IONS

Energy-loss corrections are particularly important for heavy ions because of their inherently high energy loss rates. For situations in which such corrections are required and the appropriate experimental energy loss data are not available, a consistent theoretical or semi-

empirical procedure must be adopted. A semiempirical method based on the calculation of equivalent absorber thickness has been developed for the determination of energy loss for heavy ions, a term arbitrarily taken to refer to nuclei having atomic number greater than that of the α particle.

In passage through an absorbing medium, a moving ion loses energy primarily through ionization and excitation of the atoms of the medium. As the ion slows down, its charge does not remain constant at the nuclear charge, but fluctuates due to the capture and loss of electrons. The principal difference in the energy loss process for light and heavy ions is the extent of the energy region over which the ion can be considered to be charge invariant. Protons and alpha particles have been found to maintain their full nuclear charge down to energies of approximately 1 MeV/amu; as the atomic number of the ion increases, charge variation begins at progressively higher energies.

There have been many theoretical treatments of the energy loss problem, dating from the pioneering work of Bohr.[41] It is convenient to express the predictions of these theoreies in a common form, with their differences confined to the dimensionless stopping number B, as

$$\frac{dE}{dx}=-\frac{4\pi e^4 z^{*2}}{m_e v^2}NB, \tag{A1}$$

where dE/dx is the stopping power of the absorbing medium for the ion, v is the ion velocity, N is the number of absorber atoms per unit volume, and m_e and e are the mass and charge of the electron. The effective ionic charge is denoted by z^*e and may be expressed in terms of the nuclear charge of the ion as $z^*e=\gamma ze$, where z is the atomic number of the ion and γ is the effective-charge parameter. The effective-charge parameter can thus take on values from zero to unity.

In the energy-loss theory of Bethe,[42] the stopping number B is given by

$$B=Z\ln(2m_e v^2/I)=ZL, \tag{A2}$$

where Z is the atomic number of the absorber, I is the mean excitation energy of the atomic electrons of the absorber, and L is the stopping number per atomic electron. Bloch[43] has shown that I can be expected to have an approximately linear dependence on Z, and this has been found experimentally to be the case over a wide range of Z. The relativistic correction to the stopping number has been given by Bethe[44] and others in terms of $\beta=v/c$ as

$$\Delta B=Z[-\ln(1-\beta^2)-\beta^2]=Z\Delta L, \tag{A3}$$

where ΔL is the relativistic correction to L.

On the basis of these results, it is reasonable to expect that dE/dx may be expressed, in general, in the form[45]

$$\frac{dE}{dx}=-(4\pi e^4/m_e)NZ\left(\frac{z}{v}\right)^2\gamma^2(v,z)\times[L(v,(\gamma z),Z)+\Delta L(v)], \tag{A4}$$

where the dependence on the presumed most important variables is shown explicitly. The calculation of stopping power is thus reduced to the equivalent problem of calculating the parameters L and γ. The basis of a semiempirical theory is the expression of a relative relationship between these parameters for different ions and media, and the establishment of criteria which determine when the relationships are valid.

The dependence of L and γ on ion velocity is complicated and not precisely known; therefore, a logical first criterion is the comparison of ions having the same velocity, or equivalently, the same value of energy per unit mass E_m. As a second criterion, the comparison will be made in the same absorber, i.e., for the same Z. The relative stopping power of a given absorber for two different ions moving with the same velocity may thus be expressed in the nonrelativistic limit as

$$\frac{(dE/dx)_1}{(dE/dx)_2}=\left[\frac{z_1\gamma(z_1)}{z_2\gamma(z_2)}\right]^2\times\left[\frac{L(\gamma z)_1}{L(\gamma z)_2}\right]. \tag{A5}$$

It will be assumed that the parameter L is independent of z, as it is in Bethe's theory, therefore the ratio of L values becomes unity. Since the stopping power and γ are relatively well known for protons, a third criterion will be the choice of the proton as a reference ion. The subscript corresponding to the heavy ion will now be dropped, and the subscript p will be taken to denote the proton. For energies above 1 MeV/amu, $\gamma=1$ for protons, and Eq. (A5) reduces to

$$dE/dx=(\gamma z)^2(dE/dx)_p. \tag{A6}$$

Although γ is not well known for heavy ions, it may be assumed that an ion will begin to capture electrons when its velocity decreases to approximately that of an electron in its own atom. Northcliffe,[46] in a study of the energy loss of heavy ions in aluminum, has a fact shown that there is apparently a universal dependence of γ on the ratio of ion velocity to the Bohr orbital velocity of the first electron, v/v_k for all heavy ions. An empirically determined formulation of this relationship is given by

$$\gamma^2=1-k\exp(-2v/v_k), \tag{A7}$$

with $k=1.85$. Agreement with this equation has been found for heavy ions in other solid absorbers and in a number of gases,[47,48] indicating that γ is strongly de-

[41] N. Bohr, Phil. Mag. **25**, 10 (1913).
[42] H. Bethe, Ann. Physik **5**, 325 (1930).
[43] F. Bloch, Z. Physik **81**, 363 (1933).
[44] H. Bethe, Z. Physik **76**, 293 (1932).
[45] L. C. Northcliffe, Ann. Rev. Nucl. Sci. **13**, 67 (1963).
[46] L. C. Northcliffe, Phys. Rev. **120**, 1744 (1960).
[47] F. W. Martin and L. C. Northcliffe, Phys. Rev. **128**, 1166 (1962).
[48] P. G. Roll and F. E. Steigert, Nucl. Phys. **17**, 54 (1960).

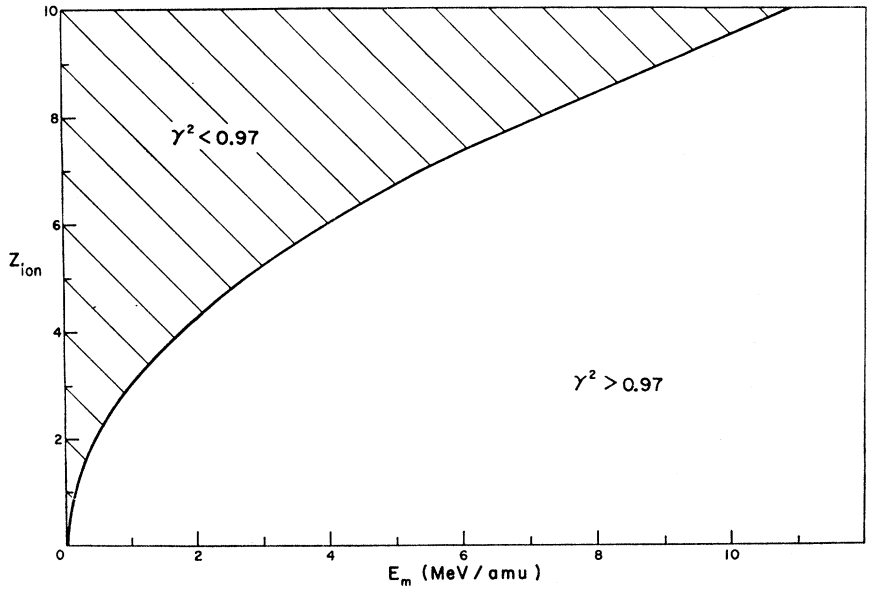

FIG. 11. The curve shown indicates ions with E_m value and atomic number z such that $\gamma^2=0.97$, where γ is the effective charge parameter. The curve is closely approximated by $E_m=z^2/9$, and the present method is expected to be applicable in the lower unshaded area.

pendent on the atomic number and velocity of the ion and relatively independent of the physical properties of the absorber.

It has been found from direct consideration of charge state population data[49] that the value of γ^2 has dropped from unity to 0.97 for O^{16} ions with $E_m=7$ MeV/amu, a situation which, according to Eq. (A7), is expected to obtain for all ions with the same value of the ratio parameter v/v_k. These ions have energies such that they lie on the curve shown in Fig. 11, which thus gives the E_m values as functions of atomic number for which $\gamma^2=0.97$. The lower unshaded portion of the figure indicates the area in ion energy-charge space for which γ^2 can be set equal to unity in Eq. (A6) with less than 3% error in the heavy ion stopping power. A final criterion will be that the method is applicable for ions whose atomic number and energy are such that they lie in this lower portion of Fig. 11. This criterion is satisfied by ions with energies given approximately by $E_m>(z^2/9)$ MeV/amu.

Under the conditions specified by the comparison criteria chosen as the basis of this method, the heavy-ion stopping power can be expressed in terms of the proton stopping power as

$$dE/dx=z^2(dE/dx)_p. \tag{A8}$$

These criteria may be summarized: (1) The heavy ion and the reference ion have the same E_m value, (2) the stopping powers of the ions are for the same absorber, (3) the reference ion is the proton, and (4) the E_m value has a lower limit given by $E_m=(z^2/9)$ MeV/amu. The critical values of E_m (MeV/amu) in (4) for several representative heavy ions are 1.8 (Be), 2.7 (B), 3.9 (C), 5.4 (N), and 7.0 (O).

[49] L. C. Northcliffe (private communication).

Heavy-ion stopping powers can be obtained from Eq. (A8) by application of a consistent set of proton stopping-power data. The proton-stopping power is given in the nonrelativistic Bethe theory of Eq. (A2), with $I/Z=$const and $\gamma z=1$, as

$$\left(\frac{dE}{dX}\right)_p=-\frac{0.24\times10^{-24}N_AZ}{AE_m}\times\left[\ln\left(\frac{E_m}{Z}\right)+c\right]\frac{\text{MeV}}{\text{mg/cm}^2}, \tag{A9}$$

where N_A is Avogadro's constant, A is the atomic weight of the absorber, and c is a parameter dependent on the absorber. The heavy-ion stopping power given in Eq. (A8) can thus be written as

$$\frac{dE}{dX}=-0.24\times10^{-24}\frac{N_AZz^2}{AE_m}\left[\ln\left(\frac{E_m}{Z}\right)+c\right]\frac{\text{MeV}}{\text{mg/cm}^2}. \tag{A10}$$

Values of the parameter c for 26 materials have been given by Whaling,[50] with additions and revisions by Demirlioglu.[51]

It should be noted that this is the electronic stopping power for the ion. The specifically nuclear stopping power has been neglected in these considerations, since a heavy ion loses a negligible amount of energy through collisions with nuclei of the absorber at the energies at which this method is expected to be applicable.

In practical applications, it is usually not the stopping power for an ion which is required, but rather the range of an ion for a given energy loss or the energy loss

[50] W. Whaling, in *Handbuch der Physik*, edited by S. Flügge (Springer-Verlag, Berlin, 1958), Vol. 34, p. 193.

[51] D. Demirlioglu and W. Whaling, California Institute of Technology report, 1962 (unpublished).

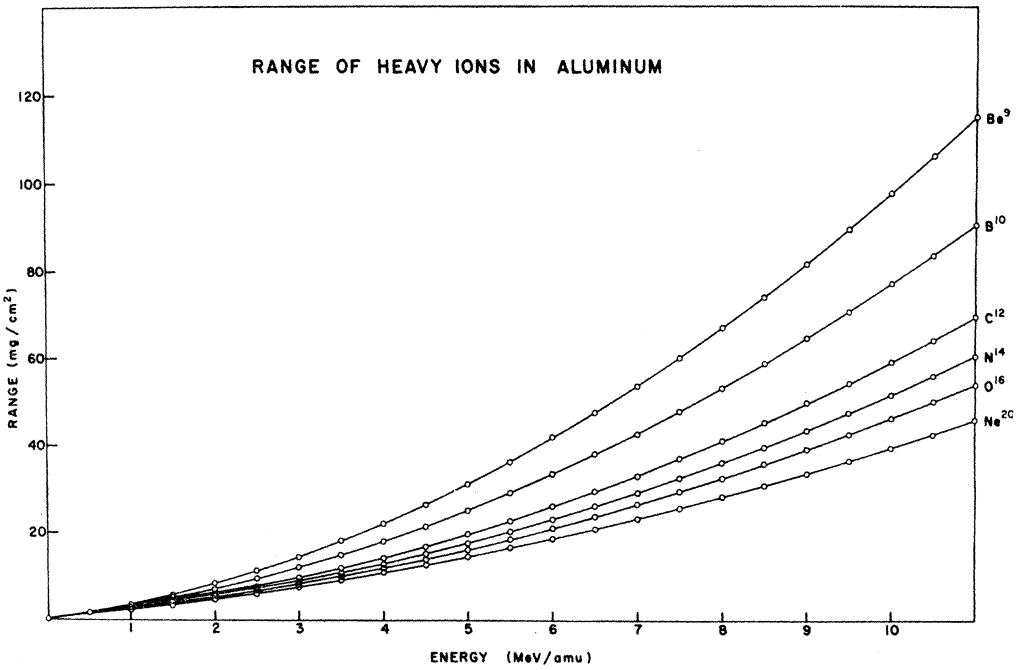

FIG. 12. Empirical range-energy relations for heavy ions in aluminum. The curves are least squares fits to the data (Ref. 52) of the function $R=a+bE+cE^2$, where R is the range in mg/cm², E is the energy in MeV/amu, and the fitting parameters a, b, and c are as given in Table III.

of an ion for a given range, i.e., a range-energy relation. Neglecting lateral displacements of the ion in the absorber and statistical fluctuations in the energy loss process, which are important only for very low ion velocities where the nuclear energy loss is significant, the range is simply given by integration of the reciprocal of the stopping power. Range-energy relations can thus be developed by numerical integration of an expression such as Eq. (A10). In the present method, however, an alternative procedure based on the calculation of equivalent absorber thickness has been adopted. The motivation for this approach was provided by the availability of a consistent, complete set of empirical range-energy relations for heavy ions in aluminum recently published by Northcliffe.[52] This technique consists of the conversion of absorber thickness to an equivalent aluminum thickness and application of these range-energy relations.

TABLE III. Empirical range-energy relations for heavy ions in aluminum. The parameters are the result of least-squares fits to the experimental data (Ref. 52) of the function $R=a+bE+cE^2$, where R is the range in mg/cm² and E is the energy in MeV/amu.

Nuclide	a	b	c
Be^9	0.070	2.715	0.705
B^{11}	0.385	2.249	0.544
C^{12}	0.439	1.855	0.404
N^{14}	0.466	1.737	0.340
O^{16}	0.482	1.696	0.290
F^{19}	0.533	1.776	0.220

[52] L. C. Northcliffe, Natl. Acad. Sci. Natl. Res. Council Publ. 1133, p. 173 (1965).

According to Eq. (A10), the ratio of the stopping powers for a heavy ion in two absorbers, denoted by subscripts 1 and 2, is given by

$$(dE/dX)_2/(dE/dX)_1=(A_1Z_2/A_2Z_1)\times[\ln(E_m/Z_2)+c_2]/[\ln(E_m/Z_1)+c_1]. \quad \text{(A11)}$$

The equivalent thickness of an absorber will be defined as the thickness of a reference absorber in which an ion loses an amount of energy equal to its energy loss in the given absorber. The equivalent thickness T for a solid absorber is therefore given in terms of its actual thickness T_0 by

$$T_{\text{solid}}=T_0(A_1Z_2/A_2Z_1)[\ln(E_m/Z_2)+c_2]/[\ln(E_m/Z_1)+c_1]\ \text{mg/cm}^2, \quad \text{(A12a)}$$

where the subscripts 1 and 2 are now associated with the reference and given absorbers, respectively. For a gas absorber, T_0 may be expressed as a constant times the atomic weight of the gas, so that

$$T_{\text{gas}}=\text{kd}(A_1Z_2/Z_1)[\ln(E_m/Z_2)+c_2]/[\ln(E_m/Z_1)+c_1]\ \text{mg/cm}^2, \quad \text{(A12b)}$$

where k is a constant containing the physical state of the gas in terms of its temperature and pressure and d is a constant equal to 2 for diatomic gases and unity otherwise. The equivalent thickness of compounds can be similarly expressed, since the molecular stopping

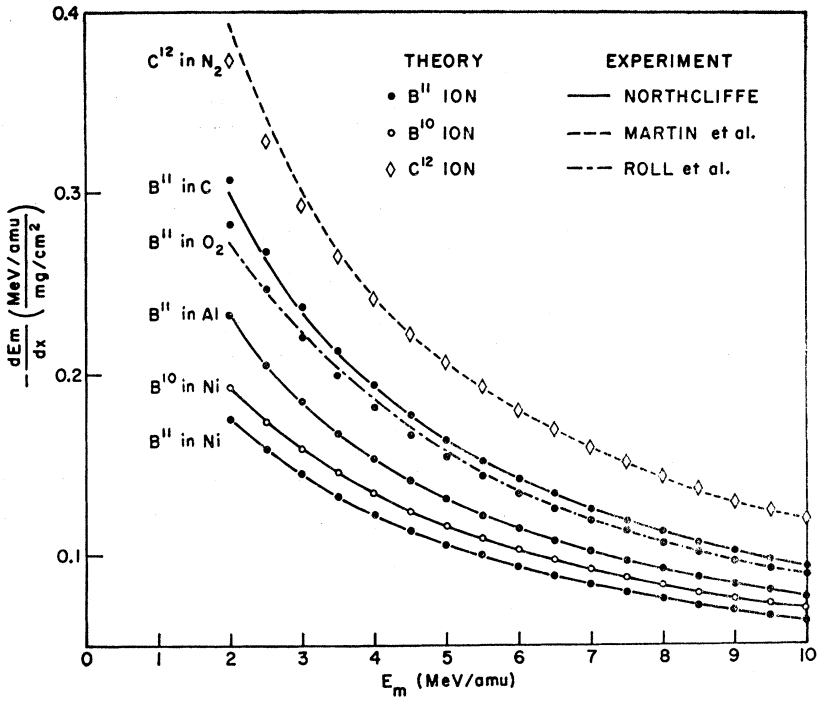

FIG. 13. Comparison of calculated and experimental stopping powers for boron and carbon ions in various materials. The curves are from the indicated experimental data (Refs. 45, 47, 48); the points are the absolute values calculated using the present theory, which is expected to be valid for $E_m > z^2/9$ MeV/amu.

power of a compound can be computed as a weighted sum of the stopping powers of its constituent atoms to a very good approximation.[50] If the reference absorber is taken to be aluminum, Eq. (A12), together with range-energy relations for heavy ions in aluminum, can be used to calculate the energy loss of any ion in any absorber for which the parameter c is known.

To facilitate the application of this procedure, the aluminum range-energy relations of Northcliffe[52] have been fitted to a three-parameter power series in the energy of the form

$$R = a + bE + cE^2, \qquad \text{(A13)}$$

where R is the range in mg/cm^2 and E_m is the energy in MeV/amu. The results of this fitting operation are shown in Fig. 12 for several representative heavy ions, and the resulting parameters are given in Table III. Ranges for other isotopes of the elements represented in Fig. 12 are in the ratio of the masses, as may be shown by a straightforward application of Eq. (A5), e.g., $R(B^{10}) = [m(B^{10})/m(B^{11})]R(B^{11})$.

To obtain the energy loss of an ion in passing through, for example, a foil window or gas target, the range in aluminum of the incident ion of given E_m value is calculated from Eq. (A13), and the equivalent thickness of the foil or target is given by Eq. (A12). The difference $R-T$ of these quantities is used in the inversion of Eq. (A13) to obtain the E_m value of the emergent ion. It has been found that this procedure is amenable to calculation by computer through coding of Eqs. (A12) and (A13) and storage of the parameters of Table III and appropriate absorber constants.

Representative calculations for boron and carbon ions in various gas and solid absorbers are compared with available experimental stopping-power data[45,47,48] in Fig. 13. The calculations are in good agreement with the experimental results in the energy region in which the method is expected to be valid.

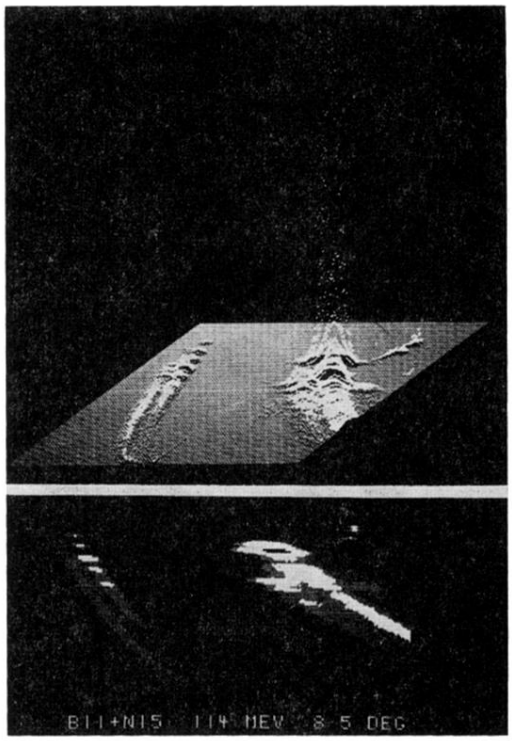

FIG. 2. Multiparameter analyzer CRT displays of dE/dx and E data from the $B^{11}+N^{15}$ reaction. The upper figure is an isometric representation of the analyzer memory, and the lower figure is a contour map of the same data. The dE/dx axis is horizontal in both displays; in each case, the loci at the left correspond to Be^{9} and Be^{10}, and those on the right correspond to B^{10}, B^{11}, and B^{12}. The peak at the extreme upper right is an artificially injected calibration pulse. In the contour display, intensity is proportional to yield, with blank areas indicating yields above maximum and below minimum thresholds; yield is shown vertically in the isometric display.